A01-31133

AIAA-2001-2530

Studies of the Continuous and Discrete Adjoint Approaches to Viscous Automatic Aerodynamic Shape Optimization

S. Nadarajah and A. Jameson
Stanford University
Stanford, CA 94305

15th AIAA Computational Fluid Dynamics Conference
June 11-14, 2001/Anaheim, CA

AIAA-2001-2530

STUDIES OF THE CONTINUOUS AND DISCRETE ADJOINT APPROACHES TO VISCOUS AUTOMATIC AERODYNAMIC SHAPE OPTIMIZATION

Siva K. Nadarajah* and Antony Jameson†
Department of Aeronautics and Astronautics
Stanford University
Stanford, California 94305 U.S.A.

Abstract

This paper compares the continuous and discrete viscous adjoint-based automatic aerodynamic optimization. The objective is to study the complexity of the discretization of the adjoint equation for both the continuous and discrete approach, the accuracy of the resulting estimate of the gradient, and its impact on the computational cost to approach an optimum solution. First, this paper presents complete formulations and discretizations of the Navier-Stokes equations, the continuous viscous adjoint equation and its counterpart the discrete viscous adjoint equation. The differences between the continuous and discrete boundary conditions are also explored. Second, the accuracy of the sensitivity derivatives obtained from continuous and discrete adjoint-based equations are compared to complex-step gradients. Third, the adjoint equations and its corresponding boundary conditions are formulated to quantify the influence of geometry modifications on the pressure distribution at an arbitrary remote location within the domain of interest. Finally, applications are presented for inverse, pressure and skin friction drag minimization, and sonic boom minimization problems.

Introduction

Computational methods have dramatically altered the design of aerospace vehicles in the last sixty years. In 1945 Lighthill[1] first proposed employing the method of conformal mapping to design two dimensional airfoils to achieve a desired target pressure distribution. These methods were restricted to incompressible flow, but later McFadden[2] extended the method to compressible flow.

Bauer et al.[3] and Garabedian et al.[4] established an alternate method by way of complex characteristics to solve the potential equations in the hodograph plane. This method successfully produced shock-free transonic flows. Constrained optimization was first attempted by Hicks et al.,[5] where they introduced the finite-difference method to evaluate the sensitivity derivatives. Since then optimization techniques for the design of aerospace vehicles have generally used gradient-based methods. Through the mathematical theory for control systems governed by partial differential equations established by Lions et al.,[6] Pironneau et al.[7] created a framework for the formulation of elliptic design problems. In the last decade, Jameson et al.[8–12] pioneered the shape optimization method for Euler and Navier-Stokes problems.

The mathematical theory for the control of systems governed by partial differential equations, as developed by Lions et al.,[6] significantly lowers the computational cost and is clearly an improvement over classical finite-difference methods. Using control theory the gradient is calculated indirectly by solving an adjoint equation. Although there is the additional overhead of solving the adjoint equation, once it has been solved the cost of obtaining the sensitivity derivatives of the cost function with respect to each design variable is negligible. Consequently, the total cost to obtain these gradients is independent of the number of design variables and amounts to the cost of one flow solution and one adjoint solution. The adjoint problem is a linear PDE of lower complexity than the flow solver. Jameson et al.[8] first applied this method to transonic flow. In the last seven years, automatic aerodynamic design of complete aircraft configurations has yielded optimized solutions of wing and wing-body configu-

*Graduate Student, Student Member AIAA

†Thomas V. Jones Professor of Engineering, Stanford University, AIAA Fellow

rations by Reuther et al.[13,14] and Burgreen et al.[15]

The continuous adjoint approach theory was developed by combining the variation of the cost function and field equations with respect to the flow-field variables and design variables through the use of Lagrange multipliers, also called costate or adjoint variables. Collecting the terms associated with the variation of the flow-field variables produces the adjoint equation and its boundary condition. The terms associated with the variation of the design variable produce the gradient. The field equations and the adjoint equation with its boundary condition must be discretized to obtain numerical solutions. As the mesh is refined, the continuous adjoint yields the exact gradient.

In the discrete adjoint approach, the control theory is applied directly to the set of discrete field equations. The discrete adjoint equation is derived by collecting together all the terms multiplied by the variation $\delta w_{i,j}$ of the discrete flow variable. If the discrete adjoint equation is solved exactly, then the resulting solution for the Lagrange multiplier produces an exact gradient of the inexact cost function and the derivatives are consistent with complex-step gradients independent of the mesh size.

A subject of on-going research is the trade-off between the complexity of the adjoint discretization, the accuracy of the resulting estimate of the gradient, and its impact on the computational cost to approach an optimum solution. Shubin and Frank[16] presented a comparison between the continuous and discrete adjoint for quasi-one-dimensional flow. A variation of the discrete field equations proved to be complex for higher order schemes. Due to this limitation of the discrete adjoint approach, early implementation of the discretization of the adjoint equation was only consistent with a first order accurate flow equation.

Burgreen et al.[15] carried a second order implementation of the discrete adjoint on three-dimensional shape optimization of wings for structured grids. For second order accuracy on unstructured grids, Elliot and Peraire[17] performed optimization on inverse pressure designs of multielement airfoils and wing-body configurations in transonic flow using a multistage Runge-Kutta scheme with Roe decomposition for the dissipative fluxes on two and three-dimensional problems. Anderson and Venkatakrishnan[18] computed inviscid and viscous optimization on unstructured grids using both the continuous and discrete adjoint. Iollo et al.[19] used the continuous adjoint approach to investigate shape optimization on one and two-dimensional flows. Ta'saan et al.[20] used a one-shot approach with the continuous adjoint formulations. Kim, Alonso, and Jameson[21] conducted an extensive gradient accuracy study of the Euler and Navier-Stokes equations which concluded that gradients from the continuous adjoint method were in close agreement with those computed by finite difference methods. A detailed comparison of the inviscid continuous and discrete adjoint approaches was conducted by Nadarajah et al.[22]

Another objective of this work is to develop the necessary methods and tools to facilitate the design of low sonic boom aircraft that can fly supersonically over land with negligible environmental impact. Traditional methods to reduce the sonic boom signature were targeted towards reducing aircraft weight, increasing lift-to-drag ratio, improving the specific fuel consumption, etc. Seebass and Argrow[23] revisited sonic boom minimization and provided a detailed study of sonic boom theory and figure of merits for the level of sonic booms. In this paper, a proof of concept of a new adjoint approach of the above problem will be demonstrated in two dimensional flow.

Objectives

1. Review the formulation and development of the viscous adjoint equations for both the continuous and discrete approach.

2. Investigate the differences in the implementation of boundary conditions for each method for various cost functions.

3. Compare the gradients of the two methods to complex step gradients for inverse pressure design and drag minimization.

4. Study the differences in calculating the exact gradient of the inexact cost function (discrete adjoint) or the inexact gradient of the exact cost function (continuous).

The Navier-Stokes Equations

In order to allow for geometric shape changes it is convenient to use a body fitted coordinate system, so that the computational domain is fixed. This requires the formulation of the Navier-Stokes equations in a transformed coordinate system. The Cartesian coordinates and velocity components are denoted by x_1, x_2, and u_1, u_2. Einstein notation simplifies the presentation of the equations, where

summation over $k = 1$ to 2 is implied by a repeated index k. The two-dimensional Navier-Stokes equations then take the form,

$$\frac{\partial w}{\partial t} + \frac{\partial f_i}{\partial x_i} = \frac{\partial f_{vi}}{\partial x_i} \quad \text{in } \mathcal{D}, \tag{1}$$

where the state vector w, inviscid flux vector f and viscous flux vector f_v are described respectively by

$$w = \begin{Bmatrix} \rho \\ \rho u_1 \\ \rho u_2 \\ \rho E \end{Bmatrix}, \quad f_i = \begin{Bmatrix} \rho u_i \\ \rho u_i u_1 + p\delta_{i1} \\ \rho u_i u_2 + p\delta_{i2} \\ \rho u_i H \end{Bmatrix}, \tag{2}$$

$$f_{vi} = \begin{Bmatrix} 0 \\ \sigma_{ij}\delta_{j1} \\ \sigma_{ij}\delta_{j2} \\ u_j\sigma_{ij} + k\frac{\partial T}{\partial x_i} \end{Bmatrix}. \tag{3}$$

In these definitions, ρ is the density, u_1, u_2 are the Cartesian velocity components, E is the total energy and δ_{ij} is the Kronecker delta function. The pressure is determined by the equation of state

$$p = (\gamma - 1)\,\rho\left\{E - \frac{1}{2}(u_i u_i)\right\},$$

and the stagnation enthalpy is given by

$$H = E + \frac{p}{\rho},$$

where γ is the ratio of the specific heats. The viscous stresses may be written as

$$\sigma_{ij} = \mu\left(\frac{\partial u_i}{\partial x_j} + \frac{\partial u_j}{\partial x_i}\right) + \lambda\delta_{ij}\frac{\partial u_k}{\partial x_k}, \tag{4}$$

where μ and λ are the first and second coefficients of viscosity. The coefficient of thermal conductivity and the temperature are computed as

$$k = \frac{c_p\mu}{Pr}, \qquad T = \frac{p}{R\rho}, \tag{5}$$

where Pr is the Prandtl number, c_p is the specific heat at constant pressure, and R is the gas constant.

For discussion of real applications using a discretization on a body conforming structured mesh, it is also useful to consider a transformation to the computational coordinates (ξ_1,ξ_2) defined by the metrics

$$K_{ij} = \left[\frac{\partial x_i}{\partial \xi_j}\right], \quad J = \det(K), \quad K_{ij}^{-1} = \left[\frac{\partial \xi_i}{\partial x_j}\right].$$

The Navier-Stokes equations can then be written in computational space as

$$\frac{\partial (Jw)}{\partial t} + \frac{\partial (F_i - F_{vi})}{\partial \xi_i} = 0 \quad \text{in } \mathcal{D}, \tag{6}$$

where the inviscid and viscous flux contributions are now defined with respect to the computational cell faces by $F_i = S_{ij}f_j$ and $F_{vi} = S_{ij}f_{vj}$, and the quantity $S_{ij} = JK_{ij}^{-1}$ represents the projection of the ξ_i cell face along the x_j axis. In obtaining equation (6) we have made use of the property that

$$\frac{\partial S_{ij}}{\partial \xi_i} = 0 \tag{7}$$

which represents the fact that the sum of the face areas over a closed volume is zero, as can be readily verified by a direct examination of the metric terms.

When equation (6) is formulated for each computational cell, a system of first-order ordinary differential equations is obtained. To eliminate odd-even decoupling of the solution and overshoots before and after shock waves, the conservative and viscous fluxes are added to a diffusion flux. The artificial dissipation scheme used in this research is a blended first and third order flux, first introduced by Jameson, Schmidt, and Turkel.[24] The artificial dissipation scheme is defined as,

$$\begin{aligned} D_{i+\frac{1}{2},j} &= \epsilon^2_{i+\frac{1}{2},j}(w_{i+1,j} - w_{i,j}) \\ &- \epsilon^4_{i+\frac{1}{2},j}(w_{i+2,j} - 3w_{i+1,j} + 3w_{i,j} - w_{i-1,j}). \end{aligned} \tag{8}$$

The first term in equation (8) is a first order scalar diffusion term, where $\epsilon^2_{i+\frac{1}{2},j}$ is scaled by the normalized second difference of the pressure and serves to damp oscillations around shock waves. $\epsilon^4_{i+\frac{1}{2},j}$ is the coefficient for the third derivative of the artificial dissipation flux. The coefficient is scaled so that it is zero at regions of large gradients, such as shock waves and eliminates odd-even decoupling elsewhere.

Formulation of the Optimal Design Problem for the Navier-Stokes Equations

It is the intent of this paper to fully investigate the derivation of both the continuous and discrete viscous adjoint method. The following information is drawn from a paper presented at the 29th AIAA Fluid Dynamics Conference, Albuquerque,[25] and repeated here to offer a comprehensive paper.

Aerodynamic optimization is based on the determination of the effect of shape modifications on some performance measure which depends on the flow. For convenience, the coordinates ξ_i describing the fixed computational domain are chosen so that each boundary conforms to a constant value of one of these coordinates. Variations in the shape then result in corresponding variations in the mapping derivatives defined by K_{ij}.

Suppose that the performance is measured by a cost function

$$I = \int_{\mathcal{B}} \mathcal{M}(w, S)\, d\mathcal{B}_\xi + \int_{\mathcal{D}} \mathcal{P}(w, S)\, d\mathcal{D}_\xi,$$

containing both boundary and field contributions where $d\mathcal{B}_\xi$ and $d\mathcal{D}_\xi$ are the surface and volume elements in the computational domain. In general, $\mathcal{M}$ and $\mathcal{P}$ will depend on both the flow variables w and the metrics S defining the computational space. In the case of a multi-point design the flow variables may be separately calculated for several different conditions of interest.

The design problem is now treated as a control problem where the boundary shape represents the control function, which is chosen to minimize I subject to the constraints defined by the flow equations (6). A shape change produces a variation in the flow solution δw and the metrics δS which in turn produce a variation in the cost function

$$\delta I = \int_{\mathcal{B}} \delta\mathcal{M}(w, S)\, d\mathcal{B}_\xi + \int_{\mathcal{D}} \delta\mathcal{P}(w, S)\, d\mathcal{D}_\xi, \quad (9)$$

with

$$\begin{aligned} \delta\mathcal{M} &= [\mathcal{M}_w]_I\, \delta w + \delta\mathcal{M}_{II}, \\ \delta\mathcal{P} &= [\mathcal{P}_w]_I\, \delta w + \delta\mathcal{P}_{II}, \end{aligned} \quad (10)$$

where we continue to use the subscripts I and II to distinguish between the contributions associated with the variation of the flow solution δw and those associated with the metric variations δS. Thus $[\mathcal{M}_w]_I$ and $[\mathcal{P}_w]_I$ represent $\frac{\partial\mathcal{M}}{\partial w}$ and $\frac{\partial\mathcal{P}}{\partial w}$ with the metrics fixed, while $\delta\mathcal{M}_{II}$ and $\delta\mathcal{P}_{II}$ represent the contribution of the metric variations δS to $\delta\mathcal{M}$ and $\delta\mathcal{P}$.

In the steady state, the constraint equation (6) specifies the variation of the state vector δw by

$$\frac{\partial}{\partial\xi_i}\delta\left(F_i - F_{vi}\right) = 0. \quad (11)$$

Here δF_i and δF_{vi} can also be split into contributions associated with δw and δS using the notation

$$\begin{aligned} \delta F_i &= [F_{iw}]_I\, \delta w + \delta F_{iII} \\ \delta F_{vi} &= [F_{viw}]_I\, \delta w + \delta F_{viII}. \end{aligned} \quad (12)$$

The inviscid contributions are easily evaluated as

$$[F_{iw}]_I = S_{ij}\frac{\partial f_j}{\partial w}, \quad \delta F_{iII} = \delta S_{ij} f_j.$$

The details of the viscous contributions are complicated by the additional level of derivatives in the stress and heat flux terms and will be derived in the following section. Multiplying by a co-state vector ψ, also known as Lagrange Multiplier, and integrating over the domain produces

$$\int_{\mathcal{D}} \psi^T \frac{\partial}{\partial\xi_i}\delta\left(F_i - F_{vi}\right) = 0. \quad (13)$$

If ψ is differentiable this may be integrated by parts to give

$$\begin{aligned} &\int_{\mathcal{B}} n_i \psi^T \delta\left(F_i - F_{vi}\right) d\mathcal{B}_\xi \\ &- \int_{\mathcal{D}} \frac{\partial\psi^T}{\partial\xi_i}\delta\left(F_i - F_{vi}\right) d\mathcal{D}_\xi = 0. \end{aligned} \quad (14)$$

Since the left hand expression equals zero, it may be subtracted from the variation in the cost function (9) to give

$$\begin{aligned} \delta I &= \int_{\mathcal{B}} \left[\delta\mathcal{M} - n_i\psi^T\delta\left(F_i - F_{vi}\right)\right] d\mathcal{B}_\xi \\ &+ \int_{\mathcal{D}} \left[\delta\mathcal{P} + \frac{\partial\psi^T}{\partial\xi_i}\delta\left(F_i - F_{vi}\right)\right] d\mathcal{D}_\xi. \end{aligned} \quad (15)$$

Now, since ψ is an arbitrary differentiable function, it may be chosen in such a way that δI no longer depends explicitly on the variation of the state vector δw. The gradient of the cost function can then be evaluated directly from the metric variations without having to re-compute the variation δw resulting from the perturbation of each design variable.

Comparing equations (10) and (12), the variation δw may be eliminated from (15) by equating all field terms with subscript "I" to produce a differential adjoint system governing ψ

$$\frac{\partial\psi^T}{\partial\xi_i}\left[F_{iw} - F_{viw}\right]_I + \mathcal{P}_w = 0 \quad \text{in } \mathcal{D}. \quad (16)$$

The corresponding adjoint boundary condition is produced by equating the subscript "I" boundary terms in equation (15) to produce

$$n_i\psi^T\left[F_{iw} - F_{viw}\right]_I = \mathcal{M}_w \quad \text{on } \mathcal{B}. \quad (17)$$

The remaining terms from equation (15) then yield a simplified expression for the variation of the cost

function which defines the gradient

$$\delta I = \int_{\mathcal{B}} \left\{ \delta \mathcal{M}_{II} - n_i \psi^T \left[\delta F_i - \delta F_{vi} \right]_{II} \right\} d\mathcal{B}_\xi + \int_{\mathcal{D}} \left\{ \delta \mathcal{P}_{II} + \frac{\partial \psi^T}{\partial \xi_i} \left[\delta F_i - \delta F_{vi} \right]_{II} \right\} d\mathcal{D}_\xi. \quad (18)$$

The details of the formula for the gradient depend on the way in which the boundary shape is parameterized as a function of the design variables, and the way in which the mesh is deformed as the boundary is modified. Using the relationship between the mesh deformation and the surface modification, the field integral is reduced to a surface integral by integrating along the coordinate lines emanating from the surface. Thus the expression for δI is finally reduced to

$$\delta I = \int_{\mathcal{B}} \mathcal{G} \delta \mathcal{F} \, d\mathcal{B}_\xi,$$

where $\mathcal{F}$ represents the design variables and $\mathcal{G}$ is the gradient, which is a function defined over the boundary surface.

The boundary conditions satisfied by the flow equations restrict the form of the left hand side of the adjoint boundary condition (17). Consequently, the boundary contribution to the cost function $\mathcal{M}$ cannot be specified arbitrarily. Instead, it must be chosen from the class of functions which allow cancellation of all terms containing δw in the boundary integral of equation (15). On the other hand, there is no such restriction on the specification of the field contribution to the cost function $\mathcal{P}$, since these terms may always be absorbed into the adjoint field equation (16) as source terms.

For simplicity, it will be assumed that the portion of the boundary that undergoes shape modifications is restricted to the coordinate surface $\xi_2 = 0$. Then equations (15) and (17) may be simplified by incorporating the conditions

$$n_1 = 0, \quad n_2 = 1, \quad d\mathcal{B}_\xi = d\xi_1,$$

so that only the variations δF_2 and δF_{v2} need to be considered at the wall boundary.

Derivation of the Viscous Continuous Adjoint Terms

This section illustrates application of control theory to aerodynamic design problems for the case of two-dimensional airfoil design using the Navier-Stokes equations as the mathematical model.

In computational coordinates, the viscous terms in the Navier–Stokes equations have the form

$$\frac{\partial F_{vi}}{\partial \xi_i} = \frac{\partial}{\partial \xi_i} \left(S_{ij} f_{vj} \right).$$

Computing the variation δw resulting from a shape modification of the boundary, introducing a Lagrange vector ψ and integrating by parts following the steps outlined by equations (11) to (14) produces

$$\int_{\mathcal{B}} \psi^T \left(\delta S_{2j} f_{vj} + S_{2j} \delta f_{vj} \right) d\mathcal{B}_\xi - \int_{\mathcal{D}} \frac{\partial \psi^T}{\partial \xi_i} \left(\delta S_{ij} f_{vj} + S_{ij} \delta f_{vj} \right) d\mathcal{D}_\xi,$$

where the shape modification is restricted to the coordinate surface $\xi_2 = 0$ so that $n_1 = 0$, and $n_2 = 1$. Furthermore, it is assumed that the boundary contributions at the far field may either be neglected or else eliminated by a proper choice of boundary conditions as previously shown for the inviscid case.[9]

The viscous terms will be derived under the assumption that the viscosity and heat conduction coefficients μ and k are essentially independent of the flow, and that their variations may be neglected. This simplification has been successfully used for many aerodynamic problems of interest. In the case of some turbulent flows, the possibility exists that the flow variations could result in significant changes in the turbulent viscosity, and it may then be necessary to account for its variation in the calculation.

Transformation to Primitive Variables

The derivation of the viscous adjoint terms is simplified by transforming to the primitive variables

$$\tilde{w}^T = (\rho, u_1, u_2, p)^T,$$

because the viscous stresses depend on the velocity derivatives $\frac{\partial u_i}{\partial x_j}$, while the heat flux can be expressed as

$$\kappa \frac{\partial}{\partial x_i} \left(\frac{p}{\rho} \right)$$

where $\kappa = \frac{k}{R} = \frac{\gamma \mu}{Pr(\gamma - 1)}$. The relationship between the conservative and primitive variations is defined by the expressions

$$\delta w = M \delta \tilde{w}, \quad \delta \tilde{w} = M^{-1} \delta w$$

which make use of the transformation matrices $M = \frac{\partial w}{\partial \tilde{w}}$ and $M^{-1} = \frac{\partial \tilde{w}}{\partial w}$. These matrices are pro-

vided in transposed form for future convenience

$$M^T = \begin{bmatrix} 1 & u_1 & u_2 & \frac{u_i u_i}{2} \\ 0 & \rho & 0 & \rho u_1 \\ 0 & 0 & \rho & \rho u_2 \\ 0 & 0 & 0 & \frac{1}{\gamma-1} \end{bmatrix}$$

$$M^{-1^T} = \begin{bmatrix} 1 & -\frac{u_1}{\rho} & -\frac{u_2}{\rho} & \frac{(\gamma-1)u_i u_i}{2} \\ 0 & \frac{1}{\rho} & 0 & -(\gamma-1)u_1 \\ 0 & 0 & \frac{1}{\rho} & -(\gamma-1)u_2 \\ 0 & 0 & 0 & \gamma-1 \end{bmatrix}.$$

The conservative and primitive adjoint operators L and $\tilde{L}$ corresponding to the variations δw and $\delta\tilde{w}$ are then related by

$$\int_{\mathcal{D}} \delta w^T L\psi \, d\mathcal{D}_\xi = \int_{\mathcal{D}} \delta\tilde{w}^T \tilde{L}\psi \, d\mathcal{D}_\xi,$$

with

$$\tilde{L} = M^T L,$$

so that after determining the primitive adjoint operator by direct evaluation of the viscous portion of (16), the conservative operator may be obtained by the transformation $L = M^{-1^T}\tilde{L}$. Since the continuity equation contains no viscous terms, it makes no contribution to the viscous adjoint system. Therefore, the derivation proceeds by first examining the adjoint operators arising from the momentum equations.

Contributions from the Momentum Equations

In order to make use of the summation convention, it is convenient to set $\psi_{j+1} = \phi_j$ for $j = 1, 2$. Then the contribution from the momentum equations is

$$\int_{\mathcal{B}} \phi_k \left(\delta S_{2j}\sigma_{kj} + S_{2j}\delta\sigma_{kj}\right) d\mathcal{B}_\xi - \int_{\mathcal{D}} \frac{\partial\phi_k}{\partial\xi_i}\left(\delta S_{ij}\sigma_{kj} + S_{ij}\delta\sigma_{kj}\right) d\mathcal{D}_\xi. \quad (19)$$

The velocity derivatives in the viscous stresses can be expressed as

$$\frac{\partial u_i}{\partial x_j} = \frac{\partial u_i}{\partial\xi_l}\frac{\partial\xi_l}{\partial x_j} = \frac{S_{lj}}{J}\frac{\partial u_i}{\partial\xi_l}$$

with corresponding variations

$$\delta\frac{\partial u_i}{\partial x_j} = \left[\frac{S_{lj}}{J}\right]_I \frac{\partial}{\partial\xi_l}\delta u_i + \left[\frac{\partial u_i}{\partial\xi_l}\right]_{II} \delta\left(\frac{S_{lj}}{J}\right).$$

The variations in the stresses are then

$$\begin{aligned}\delta\sigma_{kj} &= \left\{\mu\left[\frac{S_{lj}}{J}\frac{\partial}{\partial\xi_l}\delta u_k + \frac{S_{lk}}{J}\frac{\partial}{\partial\xi_l}\delta u_j\right] + \lambda\left[\delta_{jk}\frac{S_{lm}}{J}\frac{\partial}{\partial\xi_l}\delta u_m\right]\right\}_I \\ &+ \left\{\mu\left[\delta\left(\frac{S_{lj}}{J}\right)\frac{\partial u_k}{\partial\xi_l} + \delta\left(\frac{S_{lk}}{J}\right)\frac{\partial u_j}{\partial\xi_l}\right] + \lambda\left[\delta_{jk}\delta\left(\frac{S_{lm}}{J}\right)\frac{\partial u_m}{\partial\xi_l}\right]\right\}_{II}.\end{aligned}$$

As before, only those terms with subscript I, which contain variations of the flow variables, need be considered further in deriving the adjoint operator. The field contributions that contain δu_i in equation (19) appear as

$$-\int_{\mathcal{D}} \frac{\partial\phi_k}{\partial\xi_i} S_{ij}\left\{\mu\left(\frac{S_{lj}}{J}\frac{\partial}{\partial\xi_l}\delta u_k + \frac{S_{lk}}{J}\frac{\partial}{\partial\xi_l}\delta u_j\right) + \lambda\delta_{jk}\frac{S_{lm}}{J}\frac{\partial}{\partial\xi_l}\delta u_m\right\} d\mathcal{D}_\xi.$$

This may be integrated by parts to yield

$$\begin{aligned}&\int_{\mathcal{D}} \delta u_k \frac{\partial}{\partial\xi_l}\left(S_{lj}S_{ij}\frac{\mu}{J}\frac{\partial\phi_k}{\partial\xi_i}\right) d\mathcal{D}_\xi \\ &+ \int_{\mathcal{D}} \delta u_j \frac{\partial}{\partial\xi_l}\left(S_{lk}S_{ij}\frac{\mu}{J}\frac{\partial\phi_k}{\partial\xi_i}\right) d\mathcal{D}_\xi \\ &+ \int_{\mathcal{D}} \delta u_m \frac{\partial}{\partial\xi_l}\left(S_{lm}S_{ij}\frac{\lambda\delta_{jk}}{J}\frac{\partial\phi_k}{\partial\xi_i}\right) d\mathcal{D}_\xi,\end{aligned}$$

where the boundary integral has been eliminated by noting that $\delta u_i = 0$ on the solid boundary. By exchanging indices, the field integrals may be combined to produce

$$\int_{\mathcal{D}} \delta u_k \frac{\partial}{\partial\xi_l} S_{lj}\left\{\mu\left(\frac{S_{ij}}{J}\frac{\partial\phi_k}{\partial\xi_i} + \frac{S_{ik}}{J}\frac{\partial\phi_j}{\partial\xi_i}\right) + \lambda\delta_{jk}\frac{S_{im}}{J}\frac{\partial\phi_m}{\partial\xi_i}\right\} d\mathcal{D}_\xi,$$

which is further simplified by transforming the inner derivatives back to Cartesian coordinates

$$\int_{\mathcal{D}} \delta u_k \frac{\partial}{\partial\xi_l} S_{lj}\left\{\mu\left(\frac{\partial\phi_k}{\partial x_j} + \frac{\partial\phi_j}{\partial x_k}\right) + \lambda\delta_{jk}\frac{\partial\phi_m}{\partial x_m}\right\} d\mathcal{D}_\xi. \quad (20)$$

The boundary contributions that contain δu_i in equation (19) may be simplified using the fact that

$$\frac{\partial}{\partial\xi_l}\delta u_i = 0 \quad \text{if} \quad l = 1$$

on the boundary $\mathcal{B}$ so that they become

$$\int_{\mathcal{B}} \phi_k S_{2j}\left\{\mu\left(\frac{S_{2j}}{J}\frac{\partial}{\partial\xi_2}\delta u_k + \frac{S_{2k}}{J}\frac{\partial}{\partial\xi_2}\delta u_j\right) + \lambda\delta_{jk}\frac{S_{2m}}{J}\frac{\partial}{\partial\xi_2}\delta u_m\right\} d\mathcal{B}_\xi. \quad (21)$$

Together (20) and (21) comprise the field and boundary contributions of the momentum equations to the viscous adjoint operator in primitive variables.

Contributions from the Energy Equation

In order to derive the contribution of the energy equation to the viscous adjoint terms it is convenient to set

$$\psi_4 = \theta, \quad Q_j = u_i \sigma_{ij} + \kappa \frac{\partial}{\partial x_j}\left(\frac{p}{\rho}\right),$$

where the temperature has been written in terms of pressure and density using (5). The contribution from the energy equation can then be written as

$$\int_{\mathcal{B}} \theta \left(\delta S_{2j} Q_j + S_{2j} \delta Q_j\right) d\mathcal{B}_\xi - \int_{\mathcal{D}} \frac{\partial \theta}{\partial \xi_i} \left(\delta S_{ij} Q_j + S_{ij} \delta Q_j\right) d\mathcal{D}_\xi. \quad (22)$$

The field contributions that contain δu_i,δp, and $\delta \rho$ in equation (22) appear as

$$-\int_{\mathcal{D}} \frac{\partial \theta}{\partial \xi_i} S_{ij} \delta Q_j d\mathcal{D}_\xi = -\int_{\mathcal{D}} \frac{\partial \theta}{\partial \xi_i} S_{ij} \left\{ \delta u_k \sigma_{kj} + u_k \delta \sigma_{kj} + \kappa \frac{S_{lj}}{J} \frac{\partial}{\partial \xi_l}\left(\frac{\delta p}{\rho} - \frac{p}{\rho}\frac{\delta \rho}{\rho}\right)\right\} d\mathcal{D}_\xi. \quad (23)$$

The term involving $\delta \sigma_{kj}$ may be integrated by parts to produce

$$\int_{\mathcal{D}} \delta u_k \frac{\partial}{\partial \xi_l} S_{lj} \left\{ \mu \left(u_k \frac{\partial \theta}{\partial x_j} + u_j \frac{\partial \theta}{\partial x_k}\right) + \lambda \delta_{jk} u_m \frac{\partial \theta}{\partial x_m}\right\} d\mathcal{D}_\xi, \quad (24)$$

where the conditions $u_i = \delta u_i = 0$ are used to eliminate the boundary integral on $\mathcal{B}$. Notice that the other term in (23) that involves δu_k need not be integrated by parts and is merely carried on as

$$-\int_{\mathcal{D}} \delta u_k \sigma_{kj} S_{ij} \frac{\partial \theta}{\partial \xi_i} d\mathcal{D}_\xi. \quad (25)$$

The terms in expression (23) that involve δp and $\delta \rho$ may also be integrated by parts to produce both a field and a boundary integral. The field integral becomes

$$\int_{\mathcal{D}} \left(\frac{\delta p}{\rho} - \frac{p}{\rho}\frac{\delta \rho}{\rho}\right) \frac{\partial}{\partial \xi_l}\left(S_{lj} S_{ij} \frac{\kappa}{J} \frac{\partial \theta}{\partial \xi_i}\right) d\mathcal{D}_\xi$$

which may be simplified by transforming the inner derivative to Cartesian coordinates

$$\int_{\mathcal{D}} \left(\frac{\delta p}{\rho} - \frac{p}{\rho}\frac{\delta \rho}{\rho}\right) \frac{\partial}{\partial \xi_l}\left(S_{lj} \kappa \frac{\partial \theta}{\partial x_j}\right) d\mathcal{D}_\xi. \quad (26)$$

The boundary integral becomes

$$\int_{\mathcal{B}} \kappa \left(\frac{\delta p}{\rho} - \frac{p}{\rho}\frac{\delta \rho}{\rho}\right) \frac{S_{2j} S_{ij}}{J} \frac{\partial \theta}{\partial \xi_i} d\mathcal{B}_\xi. \quad (27)$$

This can be simplified by transforming the inner derivative to Cartesian coordinates

$$\int_{\mathcal{B}} \kappa \left(\frac{\delta p}{\rho} - \frac{p}{\rho}\frac{\delta \rho}{\rho}\right) \frac{S_{2j}}{J} \frac{\partial \theta}{\partial x_j} d\mathcal{B}_\xi, \quad (28)$$

and identifying the normal derivative at the wall

$$\frac{\partial}{\partial n} = S_{2j} \frac{\partial}{\partial x_j}, \quad (29)$$

and the variation in temperature

$$\delta T = \frac{1}{R}\left(\frac{\delta p}{\rho} - \frac{p}{\rho}\frac{\delta \rho}{\rho}\right),$$

to produce the boundary contribution

$$\int_{\mathcal{B}} k \delta T \frac{\partial \theta}{\partial n} d\mathcal{B}_\xi. \quad (30)$$

This term vanishes if T is constant on the wall but persists if the wall is adiabatic.

There is also a boundary contribution left over from the first integration by parts (22) which has the form

$$\int_{\mathcal{B}} \theta \delta \left(S_{2j} Q_j\right) d\mathcal{B}_\xi, \quad (31)$$

where

$$Q_j = k \frac{\partial T}{\partial x_j},$$

since $u_i = 0$. Notice that for future convenience in discussing the adjoint boundary conditions resulting from the energy equation, both the δw and δS terms corresponding to subscript classes I and II are considered simultaneously. If the wall is adiabatic

$$\frac{\partial T}{\partial n} = 0,$$

so that using (29),

$$\delta\left(S_{2j} Q_j\right) = 0,$$

and both the δw and δS boundary contributions vanish.

On the other hand, if T is constant $\frac{\partial T}{\partial \xi_l} = 0$ for $l = 1$, so that

$$Q_j = k\frac{\partial T}{\partial x_j} = k\left(\frac{S_{lj}}{J}\frac{\partial T}{\partial \xi_l}\right) = k\left(\frac{S_{2j}}{J}\frac{\partial T}{\partial \xi_2}\right).$$

Thus, the boundary integral (31) becomes

$$\int_{\mathcal{B}} k\theta\left\{\frac{{S_{2_j}}^2}{J}\frac{\partial}{\partial \xi_2}\delta T + \delta\left(\frac{{S_{2_j}}^2}{J}\right)\frac{\partial T}{\partial \xi_2}\right\} d\mathcal{B}_\xi \,. \quad (32)$$

Therefore, for constant T, the first term corresponding to variations in the flow field contributes to the adjoint boundary operator and the second set of terms corresponding to metric variations contribute to the cost function gradient.

All together, the contributions from the energy equation to the viscous adjoint operator are the three field terms (24), (25) and (26), and either of two boundary contributions (30) or (32), depending on whether the wall is adiabatic or has constant temperature.

The Viscous Adjoint Field Operator

Collecting together the contributions from the momentum and energy equations, the viscous adjoint operator in primitive variables can be expressed as

$$\begin{aligned}
(\tilde{L}\psi)_1 &= -\frac{p}{\rho^2}\frac{\partial}{\partial \xi_l}\left(S_{lj}\kappa\frac{\partial \theta}{\partial x_j}\right) \\
(\tilde{L}\psi)_{i+1} &= \frac{\partial}{\partial \xi_l}\left\{S_{lj}\left[\mu\left(\frac{\partial \phi_i}{\partial x_j} + \frac{\partial \phi_j}{\partial x_i}\right) + \lambda\delta_{ij}\frac{\partial \phi_k}{\partial x_k}\right]\right\} \\
&+ \frac{\partial}{\partial \xi_l}\left\{S_{lj}\left[\mu\left(u_i\frac{\partial \theta}{\partial x_j} + u_j\frac{\partial \theta}{\partial x_i}\right) + \lambda\delta_{ij}u_k\frac{\partial \theta}{\partial x_k}\right]\right\} \\
&- \sigma_{ij}S_{lj}\frac{\partial \theta}{\partial \xi_l} \qquad \text{for} \quad i = 1,2 \\
(\tilde{L}\psi)_4 &= \frac{1}{\rho}\frac{\partial}{\partial \xi_l}\left(S_{lj}\kappa\frac{\partial \theta}{\partial x_j}\right).
\end{aligned}$$

The conservative viscous adjoint operator may now be obtained by the transformation

$$L = M^{-1^T}\tilde{L}.$$

Derivation of the Viscous Discrete Adjoint Terms

The discrete adjoint equation is obtained by applying control theory directly to the set of discrete field equations. The resulting equation depends on the type of scheme used to solve the flow equations. This paper uses a cell-centered multigrid scheme with upwind-biased blended first and third order fluxes as the artificial dissipation scheme. A full discretization of the equation would involve discretizing every term that is a function of the state vector.

$$\delta I = \delta I_c + \sum_{i=2}^{nx}\sum_{j=2}^{ny}\psi_{i,j}^T\delta\left[\mathcal{R}(w) + \mathcal{D}(w) + \mathcal{V}(w)\right]_{i,j} \quad (33)$$

where δI_c is the discrete cost function, $\mathcal{R}(w)$ is the field equation, $\mathcal{D}(w)$ is the artificial dissipation term, and $\mathcal{V}(w)$ are the viscous terms.

The discrete viscous adjoint equation can be cast as such,

$$V\frac{\partial \psi_{i,j}}{\partial t} = \mathcal{R}(\psi) + \mathcal{D}(\psi) + \mathcal{V}(\psi). \quad (34)$$

Terms multiplied by the variation $\delta w_{i,j}$ of the discrete flow variables are collected and the following is the resulting convective flux of the discrete adjoint equation,

$$\begin{aligned}
&\mathcal{R}(\psi) = \\
&\left(\Delta y_{\eta_{i+\frac{1}{2},j}}\left[\frac{\partial f}{\partial w}\right]_{i,j}^T - \Delta x_{\eta_{i+\frac{1}{2},j}}\left[\frac{\partial g}{\partial w}\right]_{i,j}^T\right)\frac{\psi_{i+1,j}}{2} \\
&-\left(\Delta y_{\eta_{i-\frac{1}{2},j}}\left[\frac{\partial f}{\partial w}\right]_{i,j}^T - \Delta x_{\eta_{i-\frac{1}{2},j}}\left[\frac{\partial g}{\partial w}\right]_{i,j}^T\right)\frac{\psi_{i-1,j}}{2} \\
&+\left(\Delta x_{\xi_{i,j+\frac{1}{2}}}\left[\frac{\partial g}{\partial w}\right]_{i,j}^T - \Delta y_{\xi_{i,j+\frac{1}{2}}}\left[\frac{\partial f}{\partial w}\right]_{i,j}^T\right)\frac{\psi_{i,j+1}}{2} \\
&-\left(\Delta x_{\xi_{i,j-\frac{1}{2}}}\left[\frac{\partial g}{\partial w}\right]_{i,j}^T - \Delta y_{\xi_{i,j-\frac{1}{2}}}\left[\frac{\partial f}{\partial w}\right]_{i,j}^T\right)\frac{\psi_{i,j-1}}{2} \\
&-\left(\Delta y_{\eta_{i+\frac{1}{2},j}}\left[\frac{\partial f}{\partial w}\right]_{i,j}^T - \Delta x_{\eta_{i+\frac{1}{2},j}}\left[\frac{\partial g}{\partial w}\right]_{i,j}^T\right)\frac{\psi_{i,j}}{2} \\
&+\left(\Delta y_{\eta_{i-\frac{1}{2},j}}\left[\frac{\partial f}{\partial w}\right]_{i,j}^T - \Delta x_{\eta_{i-\frac{1}{2},j}}\left[\frac{\partial g}{\partial w}\right]_{i,j}^T\right)\frac{\psi_{i,j}}{2} \\
&-\left(\Delta x_{\xi_{i,j+\frac{1}{2}}}\left[\frac{\partial g}{\partial w}\right]_{i,j}^T - \Delta y_{\xi_{i,j+\frac{1}{2}}}\left[\frac{\partial f}{\partial w}\right]_{i,j}^T\right)\frac{\psi_{i,j}}{2} \\
&+\left(\Delta x_{\xi_{i,j-\frac{1}{2}}}\left[\frac{\partial g}{\partial w}\right]_{i,j}^T - \Delta y_{\xi_{i,j-\frac{1}{2}}}\left[\frac{\partial f}{\partial w}\right]_{i,j}^T\right)\frac{\psi_{i,j}}{2}
\end{aligned} \quad (35)$$

and

$$\mathcal{D}(\psi) = \delta d_{i+\frac{1}{2},j} - \delta d_{i-\frac{1}{2},j} + \delta d_{i,j+\frac{1}{2}} - \delta d_{i,j-\frac{1}{2}}$$

where,

$$\begin{aligned}\delta d_{i+\frac{1}{2},j} &= \epsilon^2_{i+\frac{1}{2},j}(\psi_{i+1,j} - \psi_{i,j}) - \epsilon^4_{i+\frac{3}{2},j}\psi_{i+2,j} \\ &+3\epsilon^4_{i+\frac{1}{2},j}(\psi_{i+1,j} - \psi_{i,j}) + \epsilon^4_{i-\frac{3}{2},j}\psi_{i-1,j}\end{aligned} \tag{37}$$

is the discrete adjoint artificial dissipation term and V is the cell area. The dissipation coefficients ϵ^2 and ϵ^4 are functions of the flow variables, but to reduce complexity they are treated as constants.

If a first order artificial dissipation equation is used, then equation (37) would reduce to the term associated with ϵ^2. In such a case, the discrete adjoint equations are completely independent of the costate variables in the cells below the wall. However, if we use the blended first and third order equation, then these values are required. As shown later, a simple zeroth order extrapolation across the wall produces good results.

Similar to the adjoint convective and dissipative fluxes, the discrete viscous adjoint flux can be obtained by collecting all terms multiplied by the primitive variables. After some lengthy algebraic manipulations, the conservative discrete viscous adjoint operator is obtained by multiplying it with the transformation matrix described in the section on *Derivation of the Viscous Continuous Adjoint Terms.* In these calculations, the eddy viscosity was calculated using the very simple Baldwin-Lomax turbulence model. The eddy viscosity coefficient is treated as a constant.

Viscous Adjoint Boundary Conditions for Inverse Design

Continuous Adjoint

In the continuous adjoint case, the boundary term that arises from the momentum equations including both the δw and δS components (19) takes the form

$$\int_{\mathcal{B}} \phi_k \delta\left(S_{2j}\sigma_{kj}\right) d\mathcal{B}_\xi.$$

Replacing the metric term with the corresponding local face area S_2 and unit normal n_j defined by

$$|S_2| = \sqrt{S_{2j}S_{2j}}, \quad n_j = \frac{S_{2j}}{|S_2|}$$

then leads to

$$\int_{\mathcal{B}} \phi_k \delta\left(|S_2| n_j \sigma_{kj}\right) d\mathcal{B}_\xi.$$

Defining the components of the surface stress as

$$\tau_k = n_j \sigma_{kj}$$

and the physical surface element

$$dS = |S_2|\, d\mathcal{B}_\xi,$$

the integral may then be split into two components

$$\int_{\mathcal{B}} \phi_k \tau_k \left|\delta S_2\right| d\mathcal{B}_\xi + \int_{\mathcal{B}} \phi_k \delta\tau_k dS, \tag{38}$$

where only the second term contains variations in the flow variables and must consequently cancel the δw terms arising in the cost function. The first term will appear in the expression for the gradient.

A general expression for the cost function that allows cancellation with terms containing $\delta\tau_k$ has the form

$$I = \int_{\mathcal{B}} \mathcal{N}(\tau) dS, \tag{39}$$

corresponding to a variation

$$\delta I = \int_{\mathcal{B}} \frac{\partial \mathcal{N}}{\partial \tau_k} \delta\tau_k dS,$$

for which cancellation is achieved by the adjoint boundary condition

$$\phi_k = \frac{\partial \mathcal{N}}{\partial \tau_k}.$$

Natural choices for $\mathcal{N}$ arise from force optimization and as measures of the deviation of the surface stresses from desired target values.

In the inverse design case, in order to control the surface pressure and normal stress one can measure the difference

$$n_j\left\{\sigma_{kj} + \delta_{kj}\left(p - p_d\right)\right\},$$

where p_d is the desired pressure. The normal component is then

$$\tau_n = n_k n_j \sigma_{kj} + p - p_d,$$

so that the measure becomes

$$\begin{aligned}\mathcal{N}(\tau) &= \frac{1}{2}\tau_n^2 \\ &= \frac{1}{2} n_l n_m n_k n_j \left\{\sigma_{lm} + \delta_{lm}\left(p - p_d\right)\right\} \\ &\cdot \left\{\sigma_{kj} + \delta_{kj}\left(p - p_d\right)\right\}.\end{aligned}$$

Defining the viscous normal stress as

$$\tau_{vn} = n_k n_j \sigma_{kj},$$

the measure can be expanded as

$$\begin{aligned}\mathcal{N}(\tau) &= \frac{1}{2}n_l n_m n_k n_j \sigma_{lm}\sigma_{kj} \\ &+ \frac{1}{2}\left(n_k n_j \sigma_{kj} + n_l n_m \sigma_{lm}\right)(p-p_d) + \frac{1}{2}(p-p_d)^2 \\ &= \frac{1}{2}\tau_{vn}^2 + \tau_{vn}(p-p_d) + \frac{1}{2}(p-p_d)^2 .\end{aligned}$$

For cancellation of the boundary terms

$$\phi_k\left(n_j\delta\sigma_{kj} + n_k\delta p\right) = \left\{n_l n_m \sigma_{lm} + n_l^2(p-p_d)\right\} n_k\left(n_j\delta\sigma_{kj} + n_k\delta p\right)$$

leading to the boundary condition

$$\phi_k = n_k\left(\tau_{vn} + p - p_d\right).$$

In the case of high Reynolds number, this is well approximated by the equations

$$\phi_k = n_k\left(p - p_d\right), \tag{40}$$

which should be compared with the single scalar equation derived for the inviscid boundary condition. In the case of an inviscid flow, choosing

$$\mathcal{N}(\tau) = \frac{1}{2}(p-p_d)^2$$

requires

$$\phi_k n_k \delta p = (p-p_d)\, n_k^2 \delta p = (p-p_d)\,\delta p \tag{41}$$

which is satisfied by equation (40), but which represents an over-specification of the boundary condition since only the single condition need be specified to ensure cancellation.

Discrete Adjoint

In the case of an inverse design, δI_c is the discrete form of equation (39). The $\delta w_{i,2}$ term is added to the corresponding term from equation (35), and the metric variation term is added to the gradient term. In contrast to the continuous adjoint, where the boundary condition appears as an update to the Lagrange multipliers in the cell below the wall, the discrete boundary condition appears as a source term in the adjoint fluxes. At cell $i,2$ the adjoint equation is as follows,

$$\begin{aligned}&V\frac{\partial\psi_{i,2}}{\partial t} = \\ &\frac{1}{2}\left[-A^T_{i-\frac{1}{2},2}\left(\psi_{i,2}-\psi_{i-1,2}\right) - A^T_{i+\frac{1}{2},2}\left(\psi_{i+1,2}-\psi_{i,2}\right)\right] \\ &+\frac{1}{2}\left[-B^T_{i,\frac{5}{2}}\left(\psi_{i,3}-\psi_{i,2}\right)\right] + \mathcal{D}(\psi) + \mathcal{V}(\psi) + \Phi_{inv}\end{aligned} \tag{42}$$

where Φ_{inv} is the source term for inverse design,

$$\Phi_{inv} = \left(-\Delta y_\xi \psi_{2_{i,2}} + \Delta x_\xi \psi_{3_{i,2}} - (p-p_T)\Delta s_i\right)\delta p_{i,2}$$

and,

$$A^T_{i+\frac{1}{2},2} = \Delta y_{\eta_{i+\frac{1}{2},2}}\left[\frac{\partial f}{\partial w}\right]^T_{i,2} - \Delta x_{\eta_{i+\frac{1}{2},2}}\left[\frac{\partial g}{\partial w}\right]^T_{i,2}$$

All the terms in equation (42) except for the source term are scaled as the square of Δx. Therefore, as the mesh width is reduced, the terms within parenthesis in the source term divided by Δs_i must approach zero as the solution reaches a steady state. One then recovers the continuous adjoint boundary condition as stated in equation (40).

Viscous Adjoint Boundary Conditions for Drag Minimization

Pressure Drag Minimization

In the continuous adjoint case, if the drag is to be minimized, then the cost function is the drag coefficient,

$$\begin{aligned}I &= C_d \\ &= \left(\frac{1}{c}\int_{Bw} C_p \frac{\partial y}{\partial\xi}d\xi\right)\cos\alpha \\ &+ \left(\frac{1}{c}\int_{Bw} -C_p\frac{\partial x}{\partial\xi}d\xi\right)\sin\alpha\end{aligned}$$

A variation in the shape causes a variation ∂p in the pressure and consequently a variation in the cost function,

$$\begin{aligned}\delta I &= \frac{1}{c}\int_{Bw} C_p\left(\frac{\partial y}{\partial\xi}\cos\alpha - \frac{\partial x}{\partial\xi}\sin\alpha\right)\partial p d\xi \\ &+ \frac{1}{c}\int_{Bw} C_p\left(\delta\left(\frac{\partial y}{\partial\xi}\right)\cos\alpha - \delta\left(\frac{\partial x}{\partial\xi}\right)\sin\alpha\right)d\xi\end{aligned} \tag{43}$$

As in the inverse design case, the first term is a function of the state vector, and therefore is incorporated into the boundary condition, where the integrand replaces the pressure difference term in equation (41) producing the following boundary condition,

$$\phi_k n_k = -\frac{1}{\frac{1}{2}\gamma P_\infty M_\infty^2}\begin{bmatrix}\cos\alpha \\ \sin\alpha\end{bmatrix} n_k \tag{44}$$

The discrete viscous adjoint boundary condition for pressure drag minimization can be easily obtained by replacing the $(p-p_T)\Delta s_i$ term in the

source term of equation (42) by the discrete form of equation (43).

Skin Friction Drag Minimization

For viscous force optimization, the cost function should measure skin friction drag. The skin friction force in the x_i direction is

$$CD_{fi} = \int_{\mathcal{B}} \sigma_{ij} dS_j = \int_{\mathcal{B}} S_{2j}\sigma_{ij} d\mathcal{B}_\xi$$

so that the force in a direction with cosines l_i has the form

$$C_{nf} = \int_{\mathcal{B}} l_i S_{2j}\sigma_{ij} d\mathcal{B}_\xi.$$

Expressed in terms of the surface stress τ_i, this corresponds to

$$C_{nf} = \int_{\mathcal{B}} l_i \tau_i dS,$$

so that basing the cost function (39) on this quantity gives

$$\mathcal{N} = l_i \tau_i.$$

Cancellation with the flow variation terms in equation (38) therefore mandates the continuous viscous adjoint boundary condition

$$\phi_k = l_k \tag{45}$$

where,

$$l_k = -\frac{1}{\frac{1}{2}\gamma P_\infty M_\infty^2}\begin{bmatrix}\cos\alpha \\ \sin\alpha\end{bmatrix}$$

If one would take the dot product of equation (45) then the resulting equation is identical to equation (44). Therefore, the continuous adjoint boundary condition for skin friction drag minimization also satisfies the pressure drag minimization cost function. This choice of boundary condition also eliminates the first term in equation (38) so that it need not be included in the gradient calculation. Notice that the choice for the first and fourth Lagrange multipliers can be arbitrarily set to zero or a zeroth order extrapolation across the wall can be adopted since equation (45) provides no suggestion for these values. The effect of this boundary condition is explored in the Results section.

Similar to the discrete viscous adjoint boundary conditions for the inverse design case and pressure drag minimization, the discrete viscous adjoint boundary condition for skin friction drag minimization appears as a source term in the adjoint fluxes. At cell $i, 2$ the adjoint source term Φ_v in the direction normal to the surface is as follows,

$$\begin{aligned}\Phi_v &= \mu_{i+\frac{1}{2},j+\frac{1}{2}}\left\{2\left[\frac{\partial\psi_3}{\partial y}\right]_{i+\frac{1}{2},j+\frac{1}{2}}\right. \\ &\quad \left. + v_{i+\frac{1}{2},j+\frac{1}{2}}\left[\frac{\partial\psi_4}{\partial y}\right]_{i+\frac{1}{2},j+\frac{1}{2}} - 2BC\Delta x_\xi \sin\alpha\right\} \\ &\quad - \lambda_{i+\frac{1}{2},j+\frac{1}{2}}\left\{\left[\frac{\partial\psi_2}{\partial x}\right]_{i+\frac{1}{2},j+\frac{1}{2}} + \left[\frac{\partial\psi_3}{\partial y}\right]_{i+\frac{1}{2},j+\frac{1}{2}}\right. \\ &\quad + u_{i+\frac{1}{2},j+\frac{1}{2}}\left[\frac{\partial\psi_4}{\partial x}\right]_{i+\frac{1}{2},j+\frac{1}{2}} \\ &\quad \left. + v_{i+\frac{1}{2},j+\frac{1}{2}}\left[\frac{\partial\psi_4}{\partial y}\right]_{i+\frac{1}{2},j+\frac{1}{2}}\right. \\ &\quad \left. - BC\left(\Delta y_\xi \cos\alpha + \Delta x_\xi \sin\alpha\right)\right\}\end{aligned}$$

where,

$$BC = \frac{1}{\frac{1}{2}\gamma P_\infty M_\infty^2}$$

Unlike its counterpart the viscous continuous adjoint skin friction minimization boundary condition, the viscous discrete adjoint provides boundary conditions for all four Lagrange multipliers.

Total Drag Minimization

Since the continuous adjoint boundary condition for skin friction drag minimization also satisfies the pressure drag minimization cost function, then equation (45) is used for total drag minimization.

In the discrete adjoint case, a combination of the source terms from the pressure drag minimization cost function and the skin friction drag minimization is used to achieve the desired effect.

Viscous Adjoint Boundary Conditions for the Calculation of Remote Sensitivities

Traditional adjoint implementations were aimed at reducing a cost function computed from the pressure distribution on the surface that is being modified. For supersonic boom minimization, however, we would like to obtain sensitivity derivatives of pressure distributions that are not collocated at the points where the geometry is being modified. In order to include the tailoring of the ground pressure signatures, it becomes necessary to compute sensitivity derivatives of the sonic boom signature with respect to a large number of design variables that affect the shape of the airfoil or aircraft.

Figure 1 illustrates the pressure contour and near field pressure distribution for a biconvex airfoil at Mach 1.5. In this example, the near field is approximately 6 chord lengths from the airfoil surface. The adjoint boundary condition developed to calculate remote sensitivities is applied along this location.

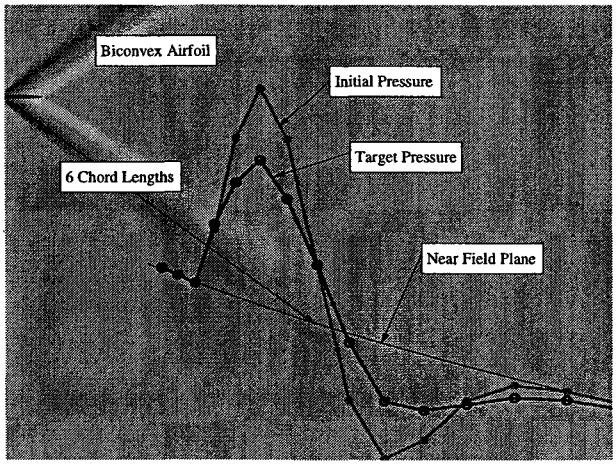

Figure 1: Pressure Contour and Near Field Pressure Distribution for Biconvex Airfoil at Mach 1.5

The weak form of the inviscid equations for steady flow can be added to the variation of the inverse pressure design cost function to yield,

$$\begin{aligned}\delta I &= \int_{B_W} (p - p_d)\,\delta p\; ds + \frac{1}{2}\int_{B_W} (p - p_d)^2\; \delta s ds \\ &- \int_{\mathcal{D}} \phi^T \frac{\partial F_k}{\partial \xi_k} d\mathcal{D}.\end{aligned}$$

The domain can then be split into two parts. First, the near field domain (NF) whose boundaries are the airfoil surface and near field boundary plane where the adjoint boundary condition will be applied. Second, the far field domain (FF) which borders the near field domain along the near field boundary plane and the far field boundary. Integrating these two field integrals by parts produces the following equation,

$$\begin{aligned}\delta I &= \int_{B_{NF}} (p - p_d)\,\delta p\; ds + \frac{1}{2}\int_{B_{NF}} (p - p_d)^2\; \delta s ds \\ &- \int_{\mathcal{D}_{NF}} \frac{\partial \psi^T}{\partial \xi_k} \delta F_k d\mathcal{D} + \int_{\mathcal{B}_W} (n_k \psi^T \delta F_k) d\mathcal{B} \\ &- \int_{\mathcal{D}_{FF}} \frac{\partial \psi^T}{\partial \xi_k} \delta F_k d\mathcal{D} + \int_{\mathcal{B}_{NF}} (n_k \psi^T \delta F_k) d\mathcal{B} \quad (46)\end{aligned}$$

The above equation contains two continuous adjoint boundary conditions. First, the fourth term in equation (46) forms the continuous adjoint wall boundary condition. Second, the first and sixth terms combine to produce the continuous adjoint boundary condition applied at the near field plane.

In the discrete adjoint case, the boundary condition for the calculation of remote sensitivities for supersonic flow is developed by adding the $\delta w_{i,NF}$ (where NF denotes the cells along the Near Field) term from the discrete cost function to the corresponding term from Eq (35). The discrete boundary condition appears as a source term in the adjoint fluxes similar to the inverse and drag minimization cases. For example, at cell (i, NF) the source term Φ_{NF} for inverse design is as follows,

$$\Phi_{NF} = -(p - p_T)\Delta s_i \delta p_{i,NF}.$$

Optimization Procedure

The search procedure used in this work is a simple descent method in which small steps are taken in the negative gradient direction. Let $\mathcal{F}$ represent the design variable, and $\mathcal{G}$ the gradient. An improvement can then be made with a shape change

$$\delta \mathcal{F} = -\lambda \mathcal{G},$$

The gradient $\mathcal{G}$ can be replaced by a smoothed value $\overline{\mathcal{G}}$ in the descent process. This ensures that each new shape in the optimization sequence remains smooth and acts as a preconditioner which allows the use of much larger steps. To apply smoothing in the ξ_1 direction, the smoothed gradient $\overline{\mathcal{G}}$ may be calculated from a discrete approximation to

$$\overline{\mathcal{G}} - \frac{\partial}{\partial \xi_1} \epsilon \frac{\partial}{\partial \xi_1} \overline{\mathcal{G}} = \mathcal{G},$$

where ϵ is the smoothing parameter. If the modification is applied on the surface $\xi_2 =$ constant, then the first order change in the cost function is

$$\begin{aligned}\delta I &= -\int\int \mathcal{G}\delta\mathcal{F} d\xi_1 \\ &= -\lambda \int\int \left(\overline{\mathcal{G}} - \frac{\partial}{\partial \xi_1}\epsilon\frac{\partial}{\partial \xi_1}\overline{\mathcal{G}}\right)\overline{\mathcal{G}} d\xi_1 \\ &= -\lambda \int\int \left(\overline{\mathcal{G}}^2 + \epsilon\left(\frac{\partial \overline{\mathcal{G}}}{\partial \xi_1}\right)^2\right) d\xi_1 \\ &< 0,\end{aligned}$$

assuring an improvement if λ is sufficiently small and positive. The smoothing leads to a large reduction

in the number of design iterations needed for convergence. An assessment of alternative search methods for a model problem is given by Jameson and Vassberg.[26]

Finite Difference Versus Complex-Step Gradients

Traditionally, finite-difference methods have been used to calculate the sensitivity derivatives of the aerodynamic cost function. The computational cost of the finite-difference method for problems involving large numbers of design variables is both unaffordable and prone to subtractive cancellation error. In order to produce an accurate finite-difference gradient, a range of step sizes must be used, and thus the ultimate cost of producing $\mathcal{N}$ gradient evaluations with the finite-difference method is a product of $m\mathcal{N}$, where m is the number of different step sizes that was used before a converged finite-difference gradient was obtained. An estimate of the first derivative of a cost function I using a first-order forward-difference approximation is as follows,

$$I^{'}(x) = \frac{I(x+h) - I(x)}{h} + \mathcal{O}(h), \qquad (47)$$

where h is the step size. A small step size is desired to reduce the truncation error $\mathcal{O}(h)$ but a very small step size would also increase subtractive cancellation errors.

Lyness and Moler introduced the use of the complex-step in calculating the derivative of an analytical function. Here, instead of using a real step h, the step size h is added to the imaginary part of the cost function. A Taylor series expansion of the cost function I yields,

$$\begin{aligned} I(x+ih) &= I(x) + ihI^{'}(x) \\ &- h^2\frac{I^{''}(x)}{2!} - ih^3\frac{I^{'''}(x)}{3!} + ... \end{aligned}$$

Take the imaginary parts of the above equation and divide by the step size h to produce a second order complex-step approximation to the first derivative

$$I^{'}(x) = \frac{\mathrm{Im[I(x+}ih)]}{h} + h^2\frac{I^{'''}(x)}{3!} + ... \qquad (48)$$

The complex step formula does not require any subtraction to yield the approximate derivative.

Figure (2) illustrates the complex-step versus the finite-difference gradient errors for the inverse design case for decreasing step sizes.

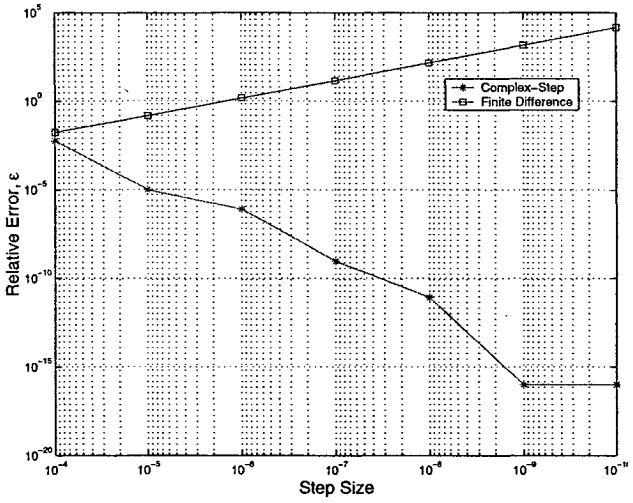

Figure 2: Complex-Step Versus Finite Difference Gradient Errors for Inverse Design Case; $\epsilon = \frac{|g-g_{ref}|}{|g_{ref}|}$

At a step size of 10^{-4} both the finite difference and complex-step approximations to the first derivative of the cost function is very similar. As the step-size is reduced, the finite-difference gradient error starts to increase instead of decreasing due to subtractive cancellation errors, however, the complex-step produces more accurate results. Therefore, the complex-step is more robust and does not require repeated calculations in order to produce an accurate gradient. If a very small step size is chosen, the gradient is calculated only once per design variable. However due to the use of double precision complex numbers, the code requires three times the wall clock time when compared to the finite difference method. But the benefits of using the complex-step to acquire accurate gradients out-weights its disadvantage.

The code used for this paper was modified to handle complex calculations using the automated method developed by Martins et al.[27]

Results

This section presents the results of the viscous inverse design, drag minimization, and sonic boom minimization cases. For each case, we compare the continuous and discrete adjoint gradients to the complex-step gradient.

Inverse Design

In an inverse design case, the target pressure is generally obtained from a known solution. The target pressure was obtained using the FLO103 flow solver for the NACA0012 airfoil at $M = 0.75$ and a lift coefficient of $C_l = 0.50$ on a 512x64 C-grid.

The design procedure is as follows. First, the flow solver module is run until at least 5 orders of magnitude drop in the residual. Second, the adjoint solver is run until at least 3 orders of magnitude drop in the residual. Next, the gradient is calculated by perturbing each point on the airfoil surface mesh. The resulting gradient is then smoothed by an implicit smoothing technique as described in the *Optimization Procedure* section. Then the airfoil geometry is updated and the grid is modified. The entire process is repeated until the conditions for optimality are satisfied. At each design iteration, 25 multigrid cycles for the flow and adjoint solver are used before the gradient is calculated. Figure (3) illustrates the design procedure.

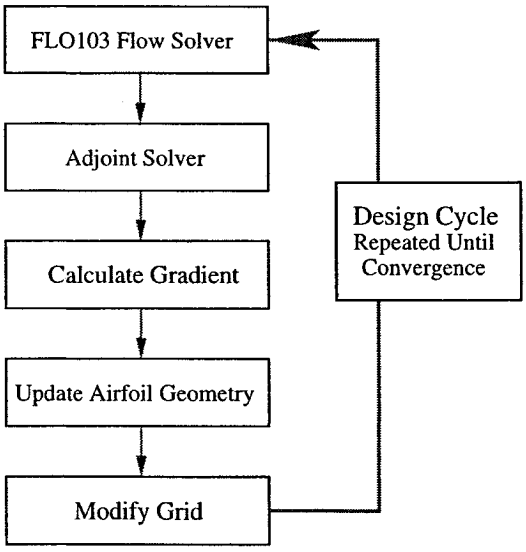

Figure 3: Design Procedure

Figure (4) illustrates an inverse design case of a NACA0012 to Onera M6 airfoil at fixed lift coefficient. Figure (4a) shows the solution for the NACA 0012 airfoil at $M = 0.75$ and $C_l = 0.50$. After only 4 design cycles, the general shape of the target airfoil is achieved as shown in figure (4b). The circles denote the target pressure distribution, the plus signs are the current upper surface pressure, and lastly, the x marks denote the lower surface pressure distribution. After 100 design iterations the desired target airfoil is obtained. Observe the point-to-point match along the shock. The figures illustrate solutions that were obtained using the continuous adjoint method. The discrete adjoint method produces identical solutions.

Figure (5) illustrates another example of an inverse design problem of a RAE to NACA 64A410 airfoil at fixed lift coefficient. Figure (5a) shows the solution for the RAE airfoil at $M = 0.75$ and $C_l = 0.50$. The final design illustrates that the target airfoil is achieved but with a slight deviation at the shock. The purpose of this example is to illustrate the successful application of the method to unsymmetric airfoils with cusped trailing edges. A very strong shock is produced on the upper surface, thus making this an ideal test case for the adjoint versus complex-step gradient comparison.

To ensure that the gradients obtained from the adjoint method is accurate: first, investigate the sensitivity of the gradient towards the convergence level of the flow and adjoint solver; and second, compare them to gradients obtained from a finite difference or complex-step method. Figure (6) illustrates the adjoint gradient errors for varying flow solver convergence. As seen in the figure, at least a 4 order magnitude drop in the flow solver convergence is required for adjoint gradients to be accurate up to 5 significant digits. Any further drop in the flow convergence has a minimal effect on the accuracy of the adjoint gradient; therefore, adjoint gradients as expected are sensitive to the convergence of the flow solver. They are not, however, sensitive towards the convergence of the adjoint solver. In figure (7) a 1 order magnitude drop in the adjoint solver produces gradients that are accurate to 4 significant digits.

Figure (8) illustrates the values of the gradients obtained from the continuous and discrete adjoint and complex-step methods. The asterisks represent the continuous adjoint gradients, the squares represent the discrete adjoint gradients, and the circles denote values that were obtained using the complex-step method. The gradient is obtained with respect to variations in Hicks-Henne sine "bump"[5] functions placed along the upper and lower surfaces of the airfoil. The figure only illustrates the values obtained

with modifications to the upper surface starting from the leading edge on the left and ending at the trailing edge on the right. The discrete adjoint equation is obtained from the discrete flow equations but without taking into account the dependence of the dissipation coefficients on the flow variables. Therefore, in order to eliminate the effect of this on comparisons with the complex-step gradient we compute the flow solution until attaining a decrease of five orders of magnitude in the residual. We then freeze the dissipative coefficients and calculate the complex-step value for each design variable.

Grid Size	Cont.	Disc.	Cont-Disc
384 x 64	$1.382e-3$	$1.331e-3$	$8.888e-5$
512 x 64	$1.008e-3$	$9.943e-4$	$4.610e-5$
1024 x 64	$7.809e-4$	$7.795e-4$	$1.425e-5$

Table 1: L_2 norm of the Difference Between Adjoint and Complex-Step Gradient

Table (1) contains values of the L_2 norm of the difference between the adjoint and complex-step gradients. The table illustrates three important facts: the difference between the discrete adjoint and the complex-step gradient is slightly smaller than that between the continuous adjoint and complex-step gradient; the norm decreases as the mesh size is increased; and the difference between continuous and discrete adjoint gradients decreases as the mesh size is increased. The second column depicts the difference between the continuous adjoint and complex-step gradient, the third column depicts the difference between the discrete adjoint and complex-step gradients, and lastly the last column depicts the difference between the discrete and continuous adjoint. As the mesh size increases, the norm of the difference between adjoint and complex-step decreases as expected. Since we derive the discrete adjoint by taking a variation of the discrete flow equations, we expect it to be consistent with the complex-step gradients and thus to be closer to the complex-step gradient than the continuous adjoint. This is confirmed by numerical results, but the difference is very small. As the mesh size increases, the difference between the continuous and discrete gradients should decrease, and this is reflected in the last column of table 1.

Drag Minimization

The drag minimization problem is broken up into three different subsections: pressure drag, skin friction drag, and total drag minimization. Figure (11) illustrates the drag minimization of RAE 2822 airfoil using the continuous adjoint formulation at a $M = 0.75$ and a fixed lift coefficient of $C_l = 0.65$. Figure (11a) shows the initial solution of the RAE 2822 airfoil with 56 drag counts due to viscous forces and 92 drag counts due to pressure drag, thus adding up to a total of 148 drag counts. In the first case, as shown in figure (11b), only the pressure drag boundary condition and its contribution towards the gradient were included. After 20 design iterations, a reduction of 50 drag counts was achieved; however, the skin friction drag increased by 1 count. In the case where only the skin friction drag boundary condition was used, a reduction of 44 drag count for the pressure drag was achieved but with no change in the skin friction drag count. As described in the section on *Continuous Adjoint Formulation*, the continuous viscous adjoint boundary condition for skin friction drag minimization satisfies the skin friction drag objective function and the pressure drag objective function. In figure (11d) the total drag was used as the objective function. The resulting airfoil has the same characteristics as the airfoil in figure (11b) that was obtained by just using the pressure drag. The skin friction drag boundary condition has not contributed towards the reduction in the skin friction drag.

Figure (12) illustrates the pressure, skin friction, and total drag minimization of the RAE 2822 airfoil using the Discrete Adjoint Formulation. In figure (12b) the airfoil was redesigned by using only the pressure drag boundary condition and its contribution towards the gradient. The solution is similar to the one obtained using the continuous adjoint boundary condition. The pressure drag was reduced by 50 drag counts, but the skin friction drag increased by two drag counts. Thus the total drag reduction is 49 drag counts, compared to the 50 that was obtained with continuous adjoint method. Figure (12c) shows the skin friction drag minimization case. Here, in contrast to the continuous adjoint where no skin friction drag was reduced, the discrete adjoint produced a reduction of 2 drag counts for the skin friction drag but the pressure drag increased by 42 drag counts. When a combination of both boundary conditions are used and their respective contributions towards the gradient are considered, then the discrete adjoint produces the exact same result as the continuous adjoint formulations. In contrast to the continuous viscous adjoint boundary condition for skin friction drag minimization, the discrete viscous adjoint boundary condition does not

satisfy the pressure drag boundary condition. Both discrete boundary conditions are independent of one from the other. This fact can be better illustrated by comparing the adjoint gradients to the complex-step gradient.

As expected, when only the pressure drag boundary condition is used, both the continuous and discrete adjoint gradients match with the complex-step gradient as shown in figure (13). Figure (14) illustrates the difference between the continuous and discrete boundary condition for skin friction drag minimization. The discrete adjoint gradient compares well with the complex-step gradient; however, the gradient produced by the continuous adjoint formulation does not compare well with the complex-step gradient. This figure illustrates why the discrete adjoint was able to reduce the skin friction drag count but not the continuous adjoint.

Figure (15) shows the gradient comparisons for the total drag minimization case. The discrete adjoint gradient is similar to the complex-step gradient, but discrepancies between the continuous and complex-step exists. These discrepancies are due to the continuous viscous adjoint boundary condition for skin friction drag minimization.

Sonic Boom Minimization

In order to validate the use of this new method for the calculation of flow sensitivities, we have constructed the following test problem, based on a biconvex airfoil with a 5% thickness ratio. For the sonic boom minimization case, the target pressure distribution was obtained by scaling down the initial near field pressure distribution at 6 chord lengths away. Figure 16 illustrates the shape of the redesigned airfoil after 100 design iterations. Only a slight modification of the lower surface of the airfoil is needed to achieve the desired near field pressure distribution. Figure 17 shows the initial near field pressure distribution. In Figure 18, the peak pressure has been reduced to almost 10% its original value after 35 design iterations. After 100 iterations, the target peak pressure is captured, as shown in Figure 19. Both the continuous and discrete viscous adjoint method produced the same result. The results shown were obtained using the discrete adjoint method.

Conclusion

This paper presents a complete formulation for the continuous and discrete adjoint approaches to automatic aerodynamic design using the Navier-Stokes equations. The gradients from each method are compared to complex-step gradients. We conclude that:

1. The continuous adjoint boundary condition appears as an update to the costate values below the wall for a cell-centered scheme, and the discrete adjoint boundary condition appears as a source term in the cell above the wall. As the mesh width is reduced, one recovers the continuous adjoint boundary condition from the discrete adjoint boundary condition.

2. The viscous continuous adjoint skin friction minimization boundary condition does not provide accurate gradients and thus failed to decrease the skin friction drag. It appears that the extrapolation of the first and fourth multipliers, as used in this work, is not adequate. However the gradients for the viscous discrete adjoint boundary condition for skin friction drag minimization does match with gradients obtained from the complex-step method and does reduce the skin friction drag.

3. Discrete adjoint gradients have better agreement than continuous adjoint gradients with complex-step gradients as expected, but the difference is generally small. (Figures 8-10)

4. As the mesh size increases, both the continuous adjoint gradients and the discrete adjoint gradients approach the complex-step gradients.

5. The difference between the continuous and discrete gradients decrease as the mesh size increases. (Tables 1)

6. The cost of deriving the discrete adjoint is greater. (Equation 35)

7. The discrete adjoint may provide a route to improving the boundary conditions for the continuous adjoint for viscous flows.

8. The best compromise may be to use the continuous adjoint formulations in the interior of the domain and the discrete adjoint boundary condition.

Acknowledgments

This research has benefitted greatly from the generous support of the AFOSR under grant number AF F49620-98-1-022.

References

[1] M.J. Lighthill A new method of two-dimensional aerodynamic design. ARC, Rand M 2112

[2] G.B. McFadden An artificial viscosity method for the design of supercritical airfoils. New York University report No. C00-3077-158.

[3] F. Bauer, P. Garabedian, D. Korn, and A. Jameson *Supercritical Wing Sections II.* Springer-Verlag, New York, 1975

[4] P. Garabedian, and D. Korn Numerical Design of Transonic Airfoils *Proceedings of SYNSPADE 1970.* pp 253-271, Academic Press, New York, 1971.

[5] R. M. Hicks and P. A. Henne. Wing Design by Numerical Optimization. *Journal of Aircraft.* 15:407-412, 1978.

[6] J.L. Lions. *Optimal Control of Systems Governed by Partial Differential Equations.* Springer-Verlag, New York, 1971. Translated by S.K. Mitter.

[7] O. Pironneau. *Optimal Shape Design for Elliptic Systems.* Springer-Verlag, New York, 1984.

[8] A. Jameson. Aerodynamic design via control theory. In *Journal of Scientific Computing*, 3:233-260,1988.

[9] A. Jameson. Automatic design of transonic airfoils to reduce the shock induced pressure drag. In *Proceedings of the 31st Israel Annual Conference on Aviation and Aeronautics, Tel Aviv*, pages 5–17, February 1990.

[10] A. Jameson. Optimum aerodynamic design using CFD and control theory. *AIAA paper 95-1729*, AIAA 12th Computational Fluid Dynamics Conference, San Diego, CA, June 1995.

[11] A. Jameson., N. Pierce, and L. Martinelli. Optimum aerodynamic design using the Navier-Stokes equations. In *AIAA 97-0101*, 35th. Aerospace Sciences Meeting and Exhibit, Reno, Nevada, January 1997.

[12] A. Jameson., L. Martinelli, and N. Pierce Optimum aerodynamic design using the Navier-Stokes equations. In *Theoretical Computational Fluid Dynamics*, 10:213-237, 1998.

[13] J. Reuther and A. Jameson. Aerodynamic shape optimization of wing and wing-body configurations using control theory. *AIAA 95-0213*, 33rd Aerospace Sciences Meeting and Exibit, Reno, Nevada, January 1995.

[14] J. Reuther, A. Jameson, J. J. Alonso, M. J Rimlinger, and D. Saunders. Constrained multipoint aerodynamic shape optimization using an adjoint formulation and parallel computers. *AIAA 97-0103*, AIAA 35th Aerospace Sciences Meeting and Exhibit, Reno, NV, January 1997.

[15] G. W. Burgreen and O. Baysal. Three-Dimensional Aerodynamic Shape Optimization of Wings Using Discrete Sensitivity Analysis. *AIAA Journal*, Vol. 34, No.9, September 1996, pp. 1761-1770.

[16] G. R. Shubin and P. D. Frank A Comparison of the Implicit Gradient Approach and the Variational Approach to Aerodynamic Design Optimization. *Boeing Computer Services Report AMS-TR-163*, April 1991.

[17] J. Elliot and J. Peraire. Aerodynamic Design Using Unstructured Meshes. *AIAA 96-1941*, 1996.

[18] W. K. Anderson and V. Venkatakrishnan Aerodynamic Design Optimization on Unstructured Grids with a Continuous Adjoint Formulation. *AIAA 96-1941*, 1996.

[19] A. Iollo, M. Salas, and S. Ta'asan. Shape Optimization Gorvened by the Euler Equations Using and Adjoint Method. *ICASE report 93-78*, November 1993.

[20] S. Ta'asan, G. Kuruvila, and M. D. Salas. Aerodynamic design and optimization in one shot. *AIAA 91-0025*, 30th Aerospace Sciences Meeting and Exibit, Reno, Nevada, January 1992.

[21] S. Kim,J. J. Alonso, and A. Jameson A Gradient Accuracy Study for the Adjoint-Based Navier-Stokes Design Method. *AIAA 99-0299*, AIAA 37th. Aerospace Sciences Meeting and Exhibit, Reno, NV, January 1999.

[22] S. Nadarajah and A. Jameson A Comparison of the Continuous and Discrete Adjoint Approach to Automatic Aerodynamic Optimization. *AIAA 00-0667*, AIAA 38th. Aerospace Sciences Meeting and Exhibit, Reno, NV, January 2000.

[23] R. Seebass, B. Argrow *Sonic Boom Minimization Revisited. AIAA paper 98-2956*, AIAA 2nd Theoretical Fluid Mechanics Meeting, Albuquerque, NM, June 1998.

[24] A. Jameson. Solution of the Euler Equations for Two Dimensional Transonic Flow By a Multigrid Method. *Applied Mathematics and Computation*, 13:327-355, 1983.

[25] A. Jameson., J. Alonso,J. Reuther,L. Martinelli, and J. Vassberg Aerodynamic Shape Optimization Techniques Based on Control Theory. *AIAA 98-2538*, AIAA 29th. Fluid Dynamics Conference, Albuquerque, NM, June 1998.

[26] A. Jameson. Studies of Alternative Numerical Optimization Methods Applied to the Brachistochrone Problem.

[27] J.R.R.A. Martins, I.M. Kroo, and J.J.Alonso An Automated Method for Sensitivity Analysis using Complex Variables. *AIAA 2000-0689*, AIAA 38th. Aerospace Sciences Meeting and Exhibit, Reno, NV, January 2000.

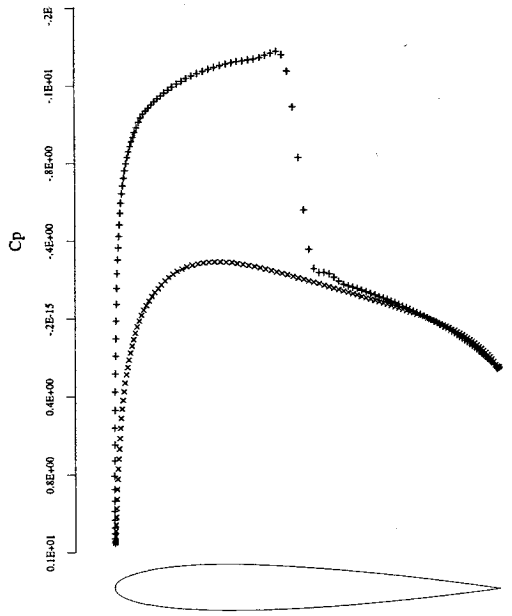

4a: Initial Solution of NACA0012 Airfoil

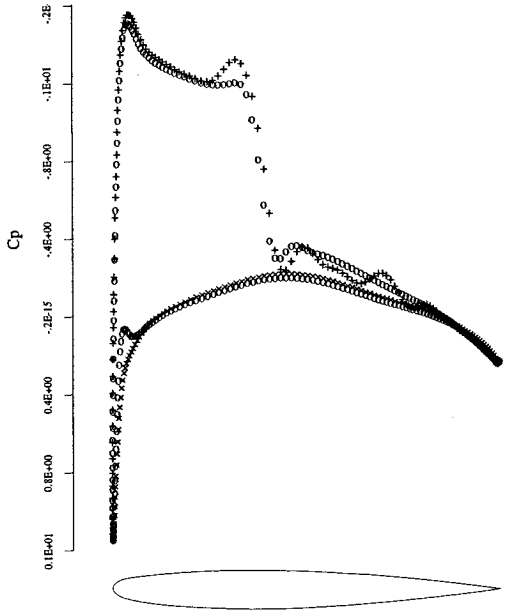

4b: After 4 Design Iterations

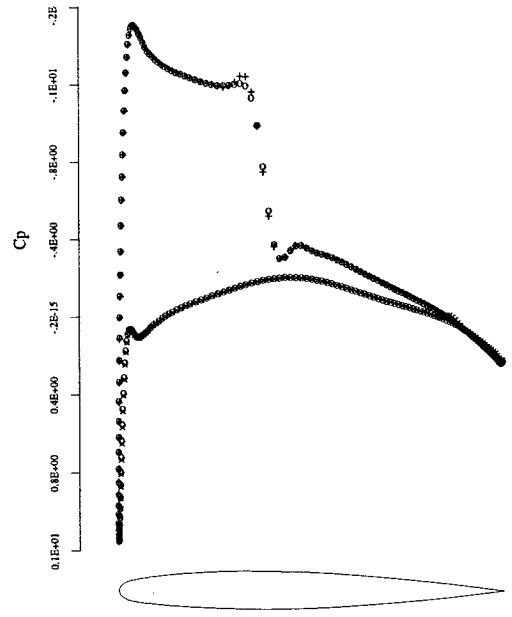

4c: After 50 Design Iterations

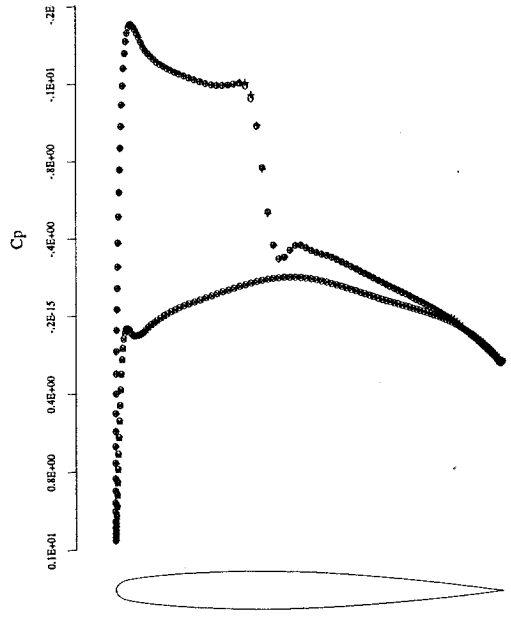

4d: Final Design after 100 Iterations

Figure 4: Inverse Design of NACA 0012 to Onera M6 at Fixed C_l
Grid - 512 x 64, $M = 0.75$, $C_l = 0.65$, $\alpha = 1$ degrees

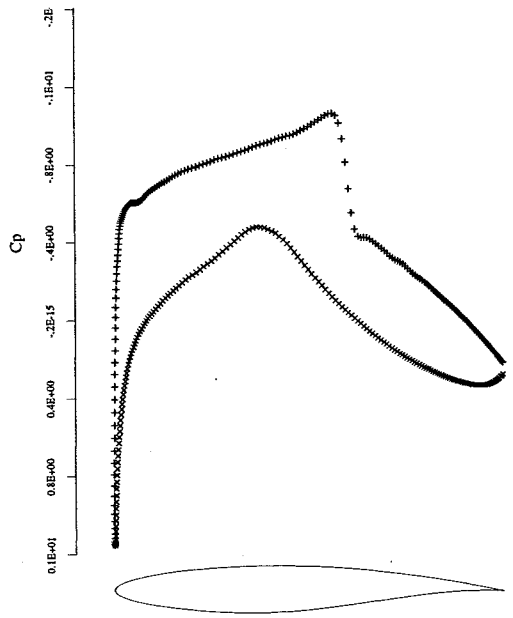

5a: Initial Solution of RAE Airfoil

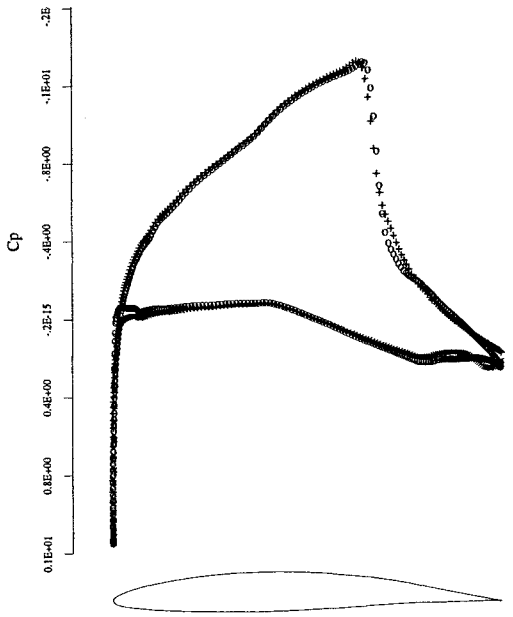

5b: After 100 Design Iterations

Figure 5: Inverse Design of RAE to NACA64A410 at Fixed C_l
Grid - 512 x 64, $M = 0.75$, $C_l = 0.50$, $\alpha = 1$ degrees

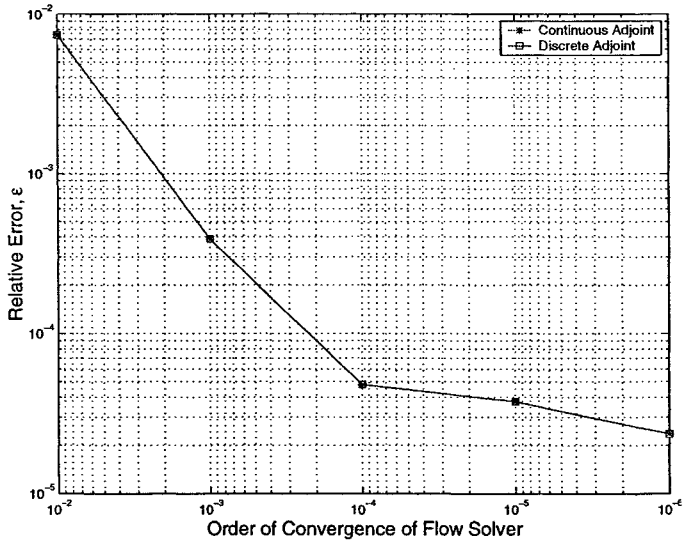

Figure 6: Adjoint Gradient Errors for Varying Flow Solver Convergence for the Inverse Design Case; $\epsilon = \frac{|g - g_{ref}|}{|g_{ref}|}$
Fine Grid - 512 x 64, $M = 0.75$, $C_l = 0.65$

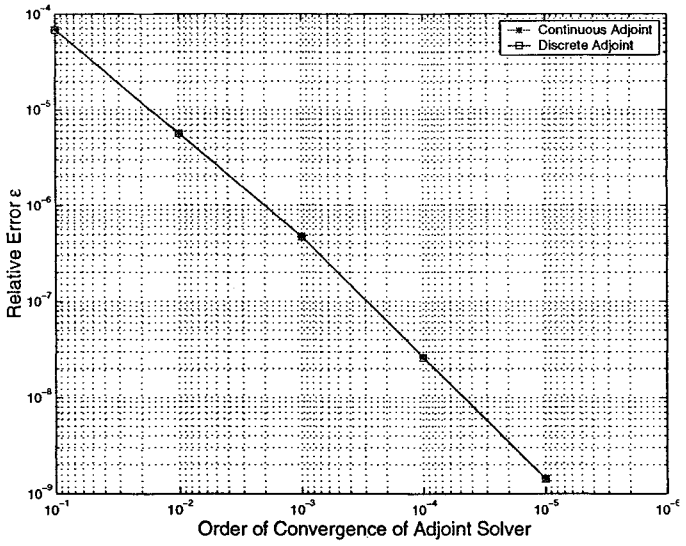

Figure 7: Adjoint Gradient Errors for Varying Adjoint Solver Convergence for the Inverse Design Case; $\epsilon = \frac{|g - g_{ref}|}{|g_{ref}|}$
Fine Grid - 512 x 64, $M = 0.75$, $C_l = 0.65$

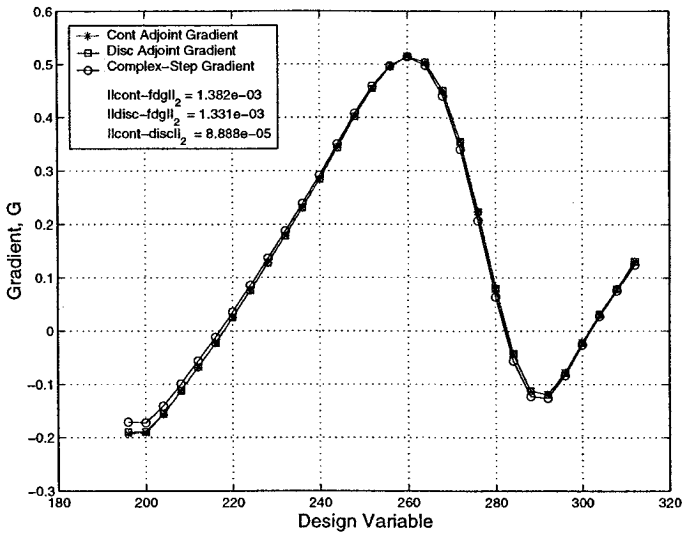

Figure 8: Adjoint Versus Complex-Step Gradients for Inverse Design of RAE to NACA64A410 at Fixed C_l.
Coarse Grid - 384 x 64, $M = 0.75$, $C_l = 0.65$

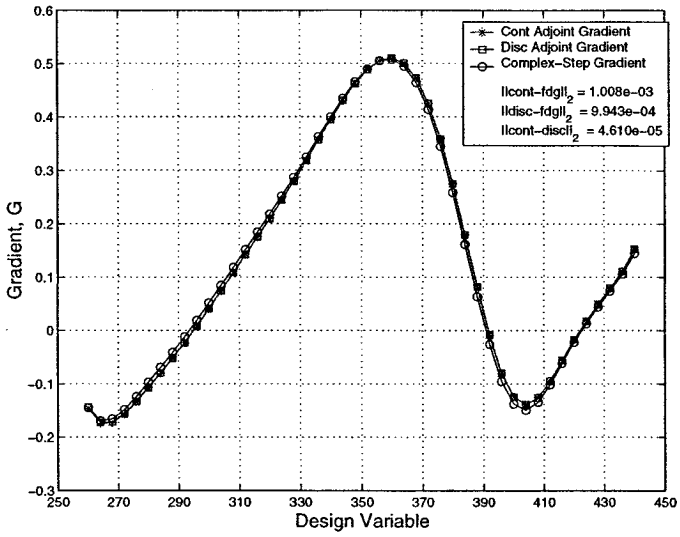

Figure 9: Adjoint Versus Complex-Step Gradients for Inverse Design of RAE to NACA64A410 at Fixed C_l.
Medium Grid - 512 x 64, $M = 0.75$, $C_l = 0.65$

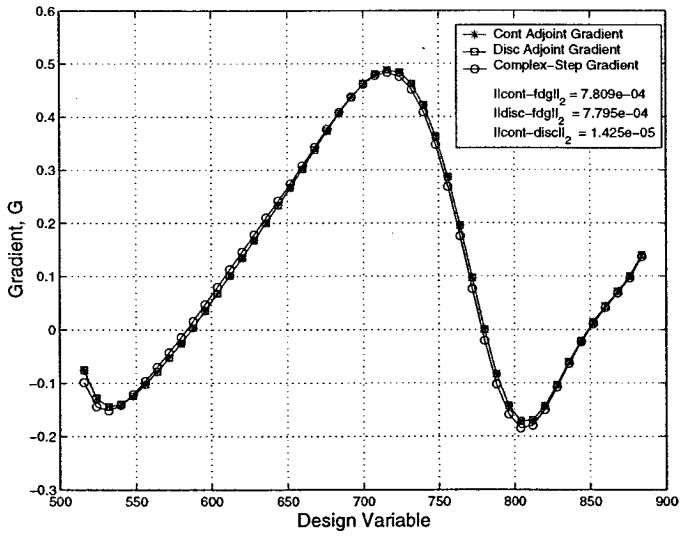

Figure 10: Adjoint Versus Complex-Step Gradients for Inverse Design of RAE to NACA64A410 at Fixed C_l.
Fine Grid - 1024 x 64, $M = 0.75$, $C_l = 0.65$

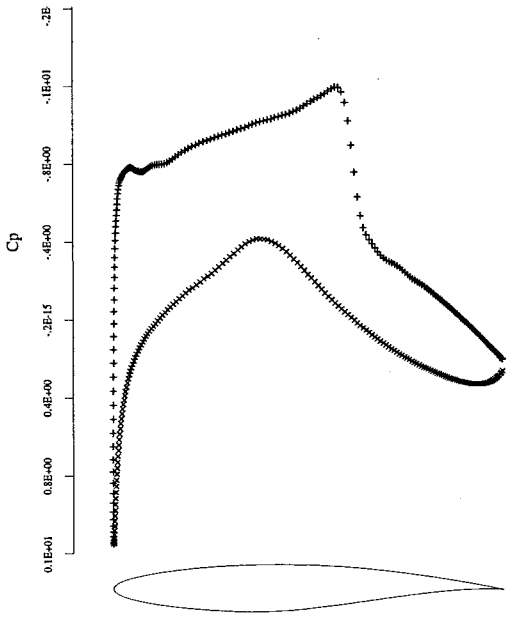

11a: Initial Solution of RAE Airfoil

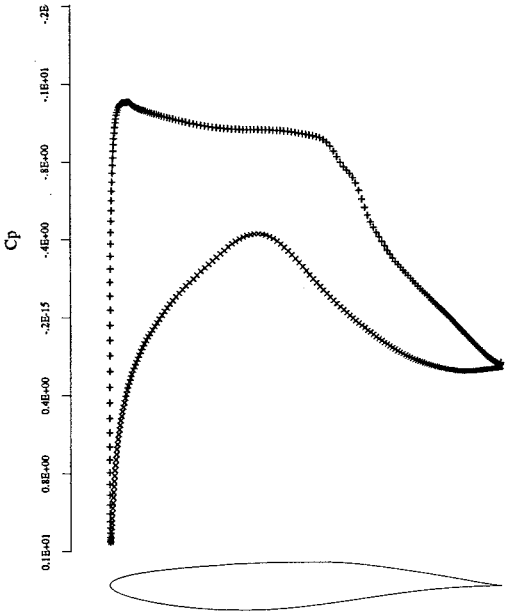

11b: Final Design Based on Pressure Drag Minimization
$C_{Dv} = .0056 \rightarrow .0057$
$C_{Total} = .0148 \rightarrow .0098$

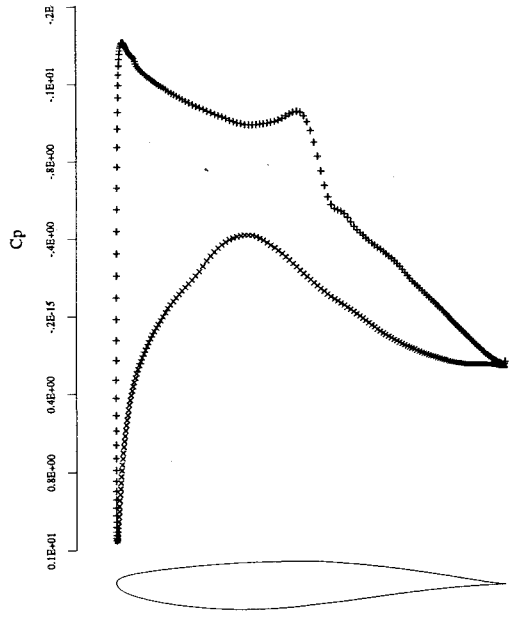

11c: Final Design Based on Viscous Drag Minimization
$C_{Dv} = .0056 \rightarrow .0056$
$C_{Total} = .0148 \rightarrow .0104$

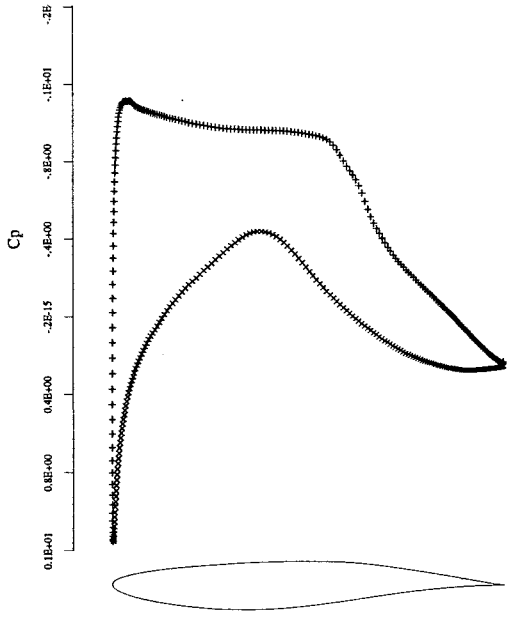

11d: Final Design Based on Total Drag Minimization
$C_{Dv} = .0056 \rightarrow .0057$
$C_{Total} = .0148 \rightarrow .0098$

Figure 11: Drag Minimization of RAE Airfoil using the Continuous Adjoint Formulation
Grid - 512 x 64, $M = 0.75$, Fixed $C_l = 0.65$, $\alpha = 1$ degrees

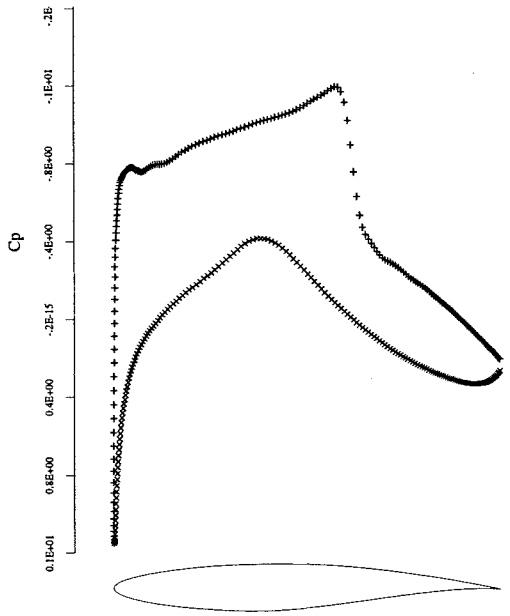

12a: Initial Solution of RAE Airfoil

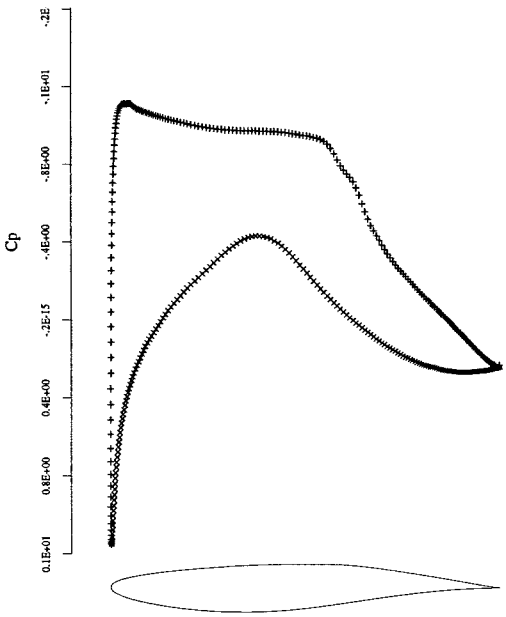

12b: Final Design Based on Pressure Drag Minimization

$C_{Dv} = .0056 \rightarrow .0058$

$C_{Total} = .0148 \rightarrow .0099$

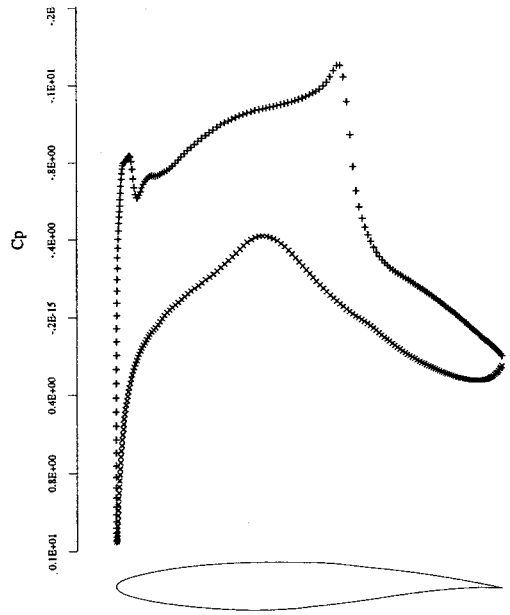

12c: Final Design Based on Viscous Drag Minimization

$C_{Dv} = .0056 \rightarrow .0054$

$C_{Total} = .0148 \rightarrow .0188$

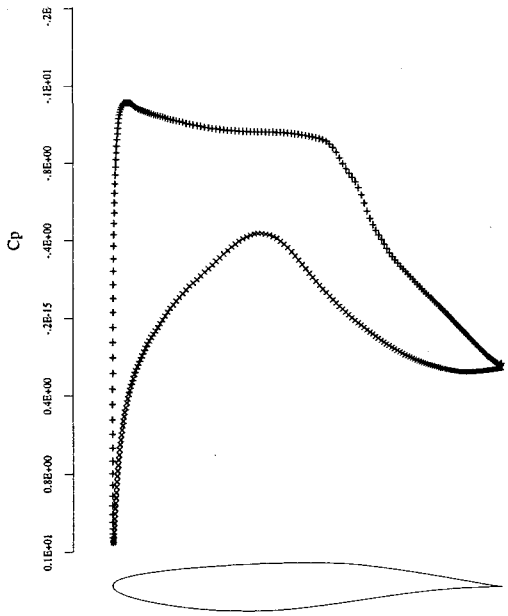

12d: Final Design Based on Total Drag Minimization

$C_{Dv} = .0056 \rightarrow .0057$

$C_{Total} = .0148 \rightarrow .0098$

Figure 12: Drag Minimization of RAE Airfoil using the Discrete Adjoint Formulation
Grid - 512 x 64, $M = 0.75$, Fixed $C_l = 0.65$, $\alpha = 1$ degrees

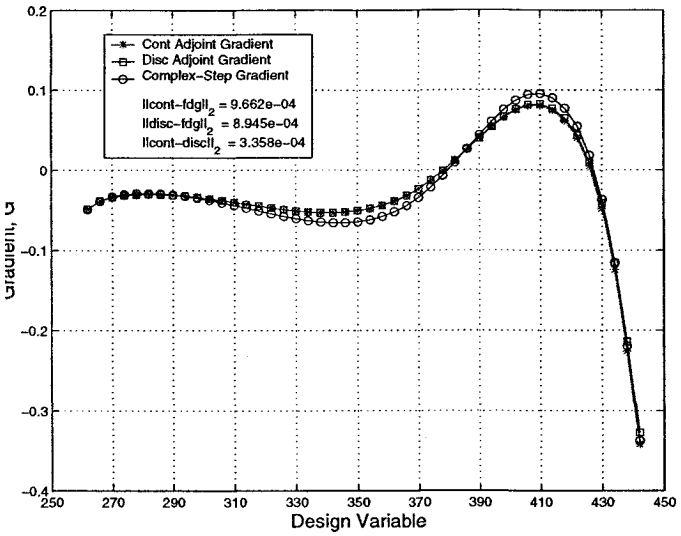

Figure 13: Adjoint Versus Complex-Step Gradients for Pressure Drag Minimization at Fixed C_l.
Fine Grid - 512 x 64, $M = 0.75$, $C_l = 0.65$

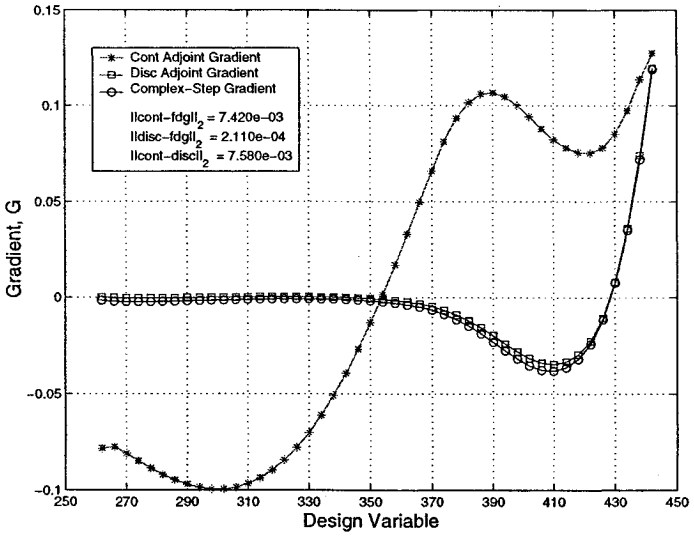

Figure 14: Adjoint Versus Complex-Step Gradients for Viscous Drag Minimization at Fixed C_l.
Fine Grid - 512 x 64, $M = 0.75$, $C_l = 0.65$

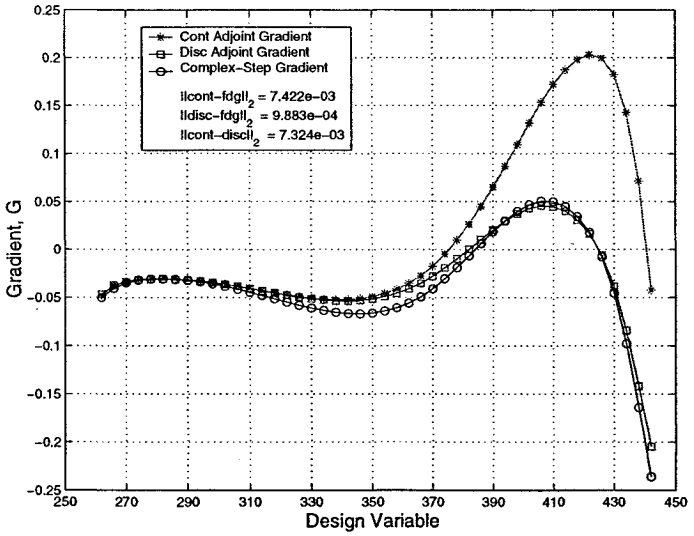

Figure 15: Adjoint Versus Complex-Step Gradients for Total Drag Minimization at Fixed C_l.
Fine Grid - 512 x 64, $M = 0.75$, $C_l = 0.65$

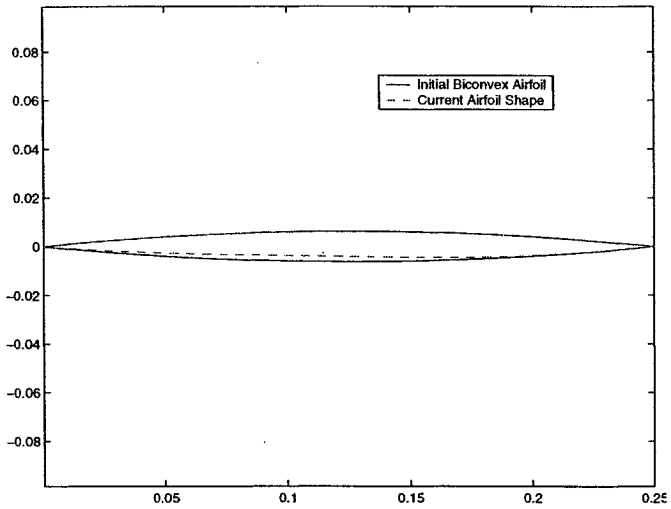

Figure 16: Sonic Boom Minimization: Initial Airfoil Shape and Final Airfoil Shape after 100 Design Iterations

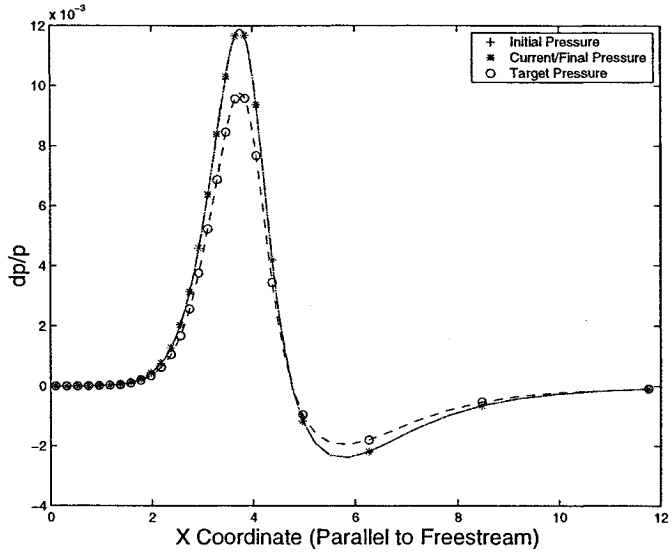

Figure 17: Sonic Boom Minimization: Initial Near Field Pressure Distribution

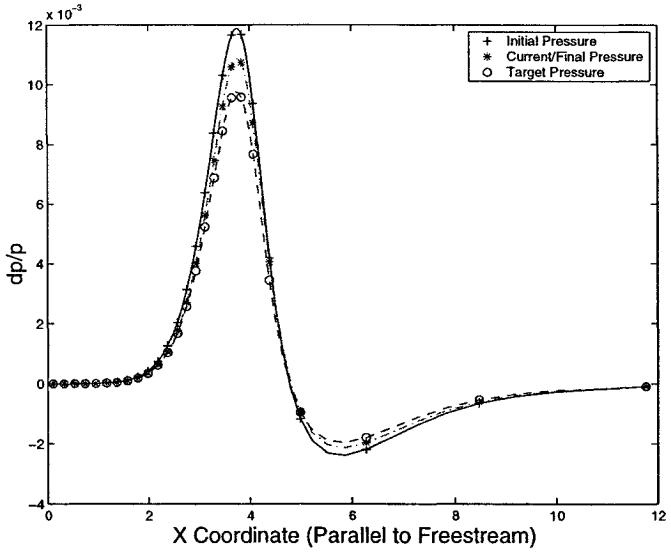

Figure 18: Sonic Boom Minimization: Pressure Distribution after 35 Design Iterations

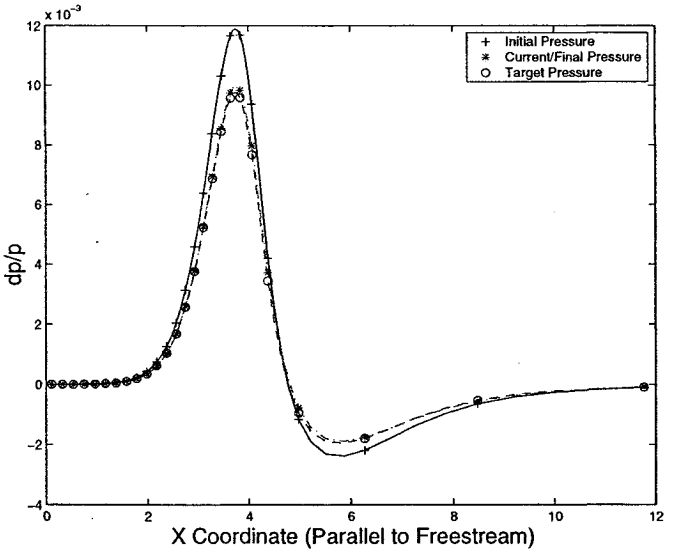

Figure 19: Sonic Boom Minimization: Pressure Distribution after 100 Design Iterations